"NOTICE: When Government or other drawings, specifications or other data are used for any purpose other than in connection with a definitely related Government procurement operation, the U.S. Government thereby incurs no responsibility, nor any obligation whatsoever; and the fact that the Government may have formulated furnished, or in any way supplied the said drawings, specifications or other data is not to be regarded by implication or otherwise as in any manner licensing the holder or any other person or corporation, or conveying any rights or permission to manufacture, use or sell any patented invention that may in any way be related thereto

T. & A. M. REPORT NO. 153

HYDROBALLISTIC CALCULATIONS OF THE RISE AND WATER EXIT OF BUOYANT BODIES

by
J. M. Robertson

November 1959

Sponsored by
Office of Naval Research
Contract Nonr 1834(01)
Project NR 062—202

DEPARTMENT OF THEORETICAL AND APPLIED MECHANICS
UNIVERSITY OF ILLINOIS

TAM Report No. 153

HYDROBALLISTIC CALCULATIONS OF THE RISE AND WATER EXIT OF BUOYANT BODIES

James M. Robertson

November 1959

Contract Nonr 1834 (10), NR 062-202

Department of Theoretical and Applied Mechanics
University of Illinois
Urbana, Illinois

ABSTRACT

Problems associated with the vertical rise and passage through a water-air interface of small buoyancy-propelled bodies are considered. In general the methods of analysis are approximate, and sometimes even crude, but the results are considered indicative of what may occur. Calculations are limited to consideration of prolate ellipsoids and usually to those of fineness ratio equal to 4. The terminal velocity and length of rise distance required to approach it closely are calculated in Chapters II and III. Comparison with experiment indicates fair agreement. It is further shown that above a diameter of 2 in. the Froude number no longer increases appreciably with body size. A rough analysis of the added-mass variation of ellipsoidal bodies as they pass through the free surface is developed in Chapter IV. This later estimate is used to indicate the expected velocity and acceleration changes of exiting bodies, in Chapter V. These are shown to diverge somewhat from those found experimentally. Besides the effect of added-mass variation, buoyancy and drag changes as the body exits are also shown to have an important effect on the velocity-distance and acceleration-distance profiles. Finally, in Chapter VI the effect of entrained water, as has been experimentally observed, is considered. Calculations of the displacement volume of the boundary layer on the body are shown to be in fair agreement with the measured entrained-water volumes. This permits some consideration of this entrainment effect at other scales of water exit occurrence -- the effects of Reynolds number and transition from laminar to turbulent boundary-layer flow are shown to be significant. Consideration of this estimate of the entrained water permits a revision in the calculated velocity and acceleration profiles; in Chapter VI this is shown to lead to closer agreement with observation. The entrained water is thus found to have an important effect on the water exit behavior of the bodies, a fact which has been suspected since the first observations of this occurrence.

TABLE OF CONTENTS

I INTRODUCTION

A study of water-exit hydroballistics as a phase of fluid-mechanics research has been underway since September 1956. Since this field is analytically difficult and relatively unexplored, the basic approach has been experimental. An earlier report (1)* describes the experimental work. In association with the experiments, certain calculations and tentative analyses have been performed to obtain indications of what can be expected. Thus the terminal velocity and rise distance calculation of Chapters II and III were needed to plan the experiments. Other calculations were made in an attempt to explain certain observed occurrences and to indicate the relative importance of the several factors entering into the water exit phenomenon.

Although admittedly inexact in some respects, the analyses presented in this report may have value for estimating expected occurrences in other situations. Thus the ballistic analysis of Chapter III may find use in other buoyant-rising-body problems. Similarly the crude water-exit analysis of Chapter IV and its use in Chapter V, besides being very suggestive for the vertical exit problem, may prove even more useful in approximate analyses of the angle exit situation. This possibility is currently being looked into.

I 1. Added Mass Effects of Exiting Bodies

When a body moves through a fluid it naturally causes a disturbance. For unsteady motions at least part of the disturbance may be treated as an effective mass of the body. The body appears to have an "added mass" of fluid moving with it. In an otherwise infinite ideal fluid, this added mass is a known function of body size and shape, although it may be difficult to calculate (2) for a body of arbitrary shape.

Experimentally and analytically this study of water exit has been concerned with bodies shaped as prolate ellipsoids (plane ellipsoids rotated about their major axes) since the added masses are well known (3) for such shapes. For analytical convenience the added mass of a body moving in a fluid is expressed as a coefficient k times the mass of fluid displaced by the body; thus, added mass equals $k\rho\forall$ (ρ is the fluid density, $\forall$ the volume of the body).

---

* Numbers in parentheses indicate references as listed on page 63.

The problem of water exit involves a body in a semi-infinite fluid. The free surface limits the liquid medium. A very simple indication of what might be expected as a buoyant body passes through a water-air interface is afforded by an elementary momentum analysis including the effect of added mass. As indicated in Fig. 1 when the body is rising with terminal velocity in water at some distance ($|y| > \ell$) below the surface, the forces acting on it must be in equilibrium, i.e., the buoyancy is exactly balanced by the weight and drag. Once it exits, the buoyancy is lost and the body quickly starts to decelerate due to the action of its weight and the air drag forces (which are small, however). But, for short while, it would appear that the body should have a larger velocity in air than it has in water. This is shown by equating the momenta of the body and added fluid before exit to those after exit.

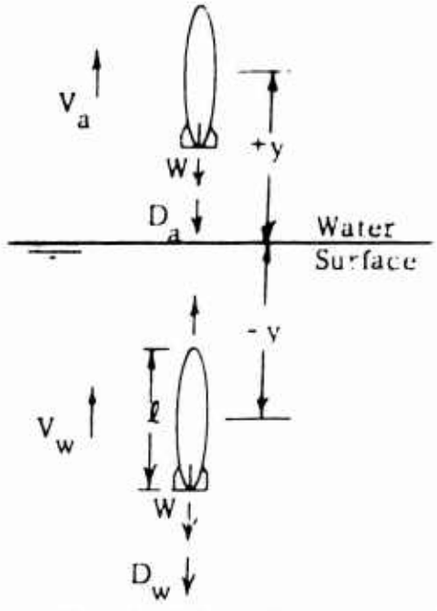

Fig. 1. Sketch of Body Before and After Exit.

Using the subscript w to indicate the situation with the body in water and a for the body in air, the momenta of the body plus added mass M' are equated in the two situations

$$(M + M'_w)\, V_w = (M + M'_a)\, V_a$$

It is assumed that the momentum which may be left in the water in the form of waves or other disturbances, after the body has exited, is relatively small and may be neglected.

Using the subscript b to designate the body, the foregoing momentum expression may be written

$$(\rho_b + k\rho_w)\, \forall\, V_w = (\rho_b + k\rho_a)\, \forall\, V_a$$

where ρ indicates the fluid density. The density of air is negligible compared with that of water. If the ratio ρ_b/ρ_w is designated as the specific gravity S of the body, then

$$\frac{V_a}{V_w} = 1 + \frac{k}{S} \qquad (1)$$

The apparently sudden increase in velocity predicted by this analysis has been referred to as the "velocity jump". As an indication of the expected magnitude of this rate, consider bodies of fineness 4 and 8. Their added mass coefficients, k (for longitudinal motion) are 0.082 and 0.029. Low specific gravity bodies are needed to obtain appreciable velocity jumps. Thus for S of 0.2, the velocities will increase by 41 and 14 percent, respectively.

The actual situation is more complicated than the simple momentum analysis would imply. The details of the occurrences as the body passes through the interface are of prime interest, but it is exactly these which are glossed over by the momentum approach. Information is needed on the variation in added mass in this situation in order to permit one to evaluate the velocities and accelerations to which the body will be subjected.

1.2 Added Masses of Bodies in Infinite Fluid

The added masses of simple bodies in an infinite ideal fluid have been calculated (3, 4). For a cylinder moving perpendicular to its axis, k is 1, but for ellipsoids moving parallel to their major axes, k varies from 0.5 for the sphere to 0.0155 for a body of fineness ratio of 12. The fineness ratios, $\ell/d = f$, of the bodies represent the ratio of their lengths, ℓ, to maximum diameters, d. The variation of k with ℓ/d has been tabulated by Lamb (1918); this together with the wetted surface area are shown as a function of ℓ/d in the Appendix (Fig. A1).

Although the added mass can be calculated in many cases or at least estimated (2) there has been little experimental check on these results. The added mass is not measureable -- at most it can be inferred from experiment. About the only determinations have been for vibrating bodies. Even the simple case of a body accelerating from rest has had little experimental verification (5). Some evidence along this line was obtained in the experimental phases of this study and was submitted in an earlier report (1), where this point was further discussed.

1.3. Added Mass Variation Near Surface

If the boundary to the semi-infinite fluid were rigid, its effect would be relatively easily analyzed. Thus hydrodynamics (3, 4) indicates that for a sphere moving perpendicular to a plane rigid surface

$$k = 0.5 \left(1 + \frac{3}{64} \frac{d^3}{y^3}\right) \qquad (2)$$

where d = diameter of sphere and y = the distance of its centroid from the surface (taken positive here). Since k increases as y decreases the effect is that of a repulsive force. For motion parallel to the surface, the added mass decreases and it appears as though there were an attractive force. The above relation for k is no longer correct even before the sphere touches the surface (y = d/2), but it is still of value in indicating the order of the effects. The indicated k is then increased by 32 percent. For a light body (S = 0.2) this would result in an 11 percent reduction in velocity, according to the velocity relation of Eq. 1.

A free surface, or interface between fluids of different density, does not usually behave as a rigid wall since it is free to deflect under the restraining influence of gravity. It is not surprising therefore that the mode of behavior can be shown to depend upon the Froude number, the ratio of inertial to gravity forces (1). It has been stated that at low Froude numbers the surface behaves as though it were rigid (velocity normal to surface zero) while at high Froude numbers the surface pressure must be constant and the surface is free to deform (zero velocity potential on surface). For the later case the added mass decreases as a body approaches normal to a free surface. This is opposite to the effect noted above for the sphere approaching a rigid wall. In the first report on this project (1) the surface behavior effects were more thoroughly discussed and reference made to the recent work of Motora (1953), Eisenberg (1955) and Breslin and Kaplan (1957). It was noted that a first-order approximation to the high-Froude number situation is found from the inverse hydrodynamic-image analysis. This leads to an expression for the added mass coefficient differing only in sign from the rigid (low Froude number) result. Thus for the sphere

$$k = 0.5\left(1 - \frac{3}{64}\frac{d^3}{y^3}\right) \qquad (2a)$$

When the sphere just touches the free surface (y = d/2), k is reduced by 50 percent to a value of 0.25. This would result in a velocity increase of 55 percent for the light body (S = 0.2) considered previously.

I.4. Some Experimental Observations

A brief indication of the nature of the observed behavior of the exiting bodies appears in order. This represents only the highlights of the results summarized in reference (1) and is included to help give this report proper perspective. The calculations of the following chapters will be compared directly with results from the experiments, where possible; in other cases the comparison will be qualitative.

The experiments have been conducted with buoyant bodies of diameters from 1 to 4 in. and fineness ratios ℓ/d of 4 and 8. A photograph of a body after exit is presented in Fig. 2. The motion of the bodies is recorded by high speed photographs. Position measurements from the films are analyzed to yield velocity and acceleration profiles. Fig. 3 presents a sample set of profiles. The velocity jump is seen to be considerably different from the prediction of the simple momentum analysis. The peak velocity occurs below the free surface and is only about 14 percent of that predicted by Eq. 1. The photograph of Fig. 2 indicates another deviation from elementary expectations -- a considerable amount of water is entrained by the body and exits with it.

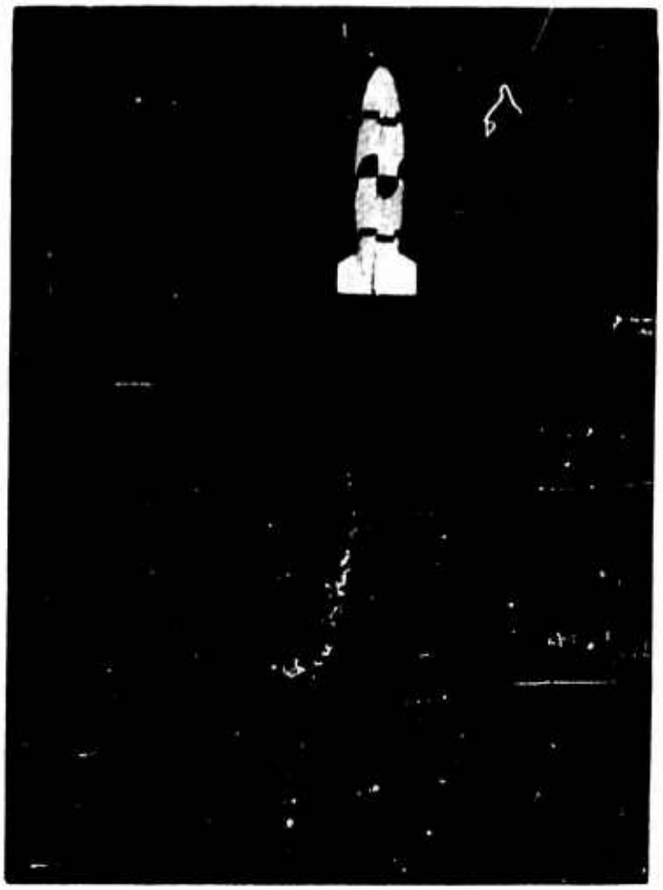

Fig. 2. Photograph of Exiting Body.

The analysis of the experimental studies reported (1), included an attempt to evaluate the added mass of the bodies as they approached the free surface. The apparent added mass of the body when its nose just touched the free surface was found to be a function of Froude number and it was possible to define the low and high Froude number ranges. Figure 4 presents the results (1) in which it appears that k decreases monotonically with increase in Froude number. A Froude number value of about 3, based on body diameter ($\mathbb{F} = V/\sqrt{gd}$) separates the two regimes.

I.5. The Problem

The preceeding discussions and the experimental results presented more completely elsewhere (1) serve to indicate the problem with which this project in general, and this report in particular, is concerned. It is apparent that rather small effects are occurring as the bodies approach and pass through the free surface. The momentum analysis is rather too crude while exact analyses based on potential theory are difficult of application, due to the necessary considerations of the free surface behavior.

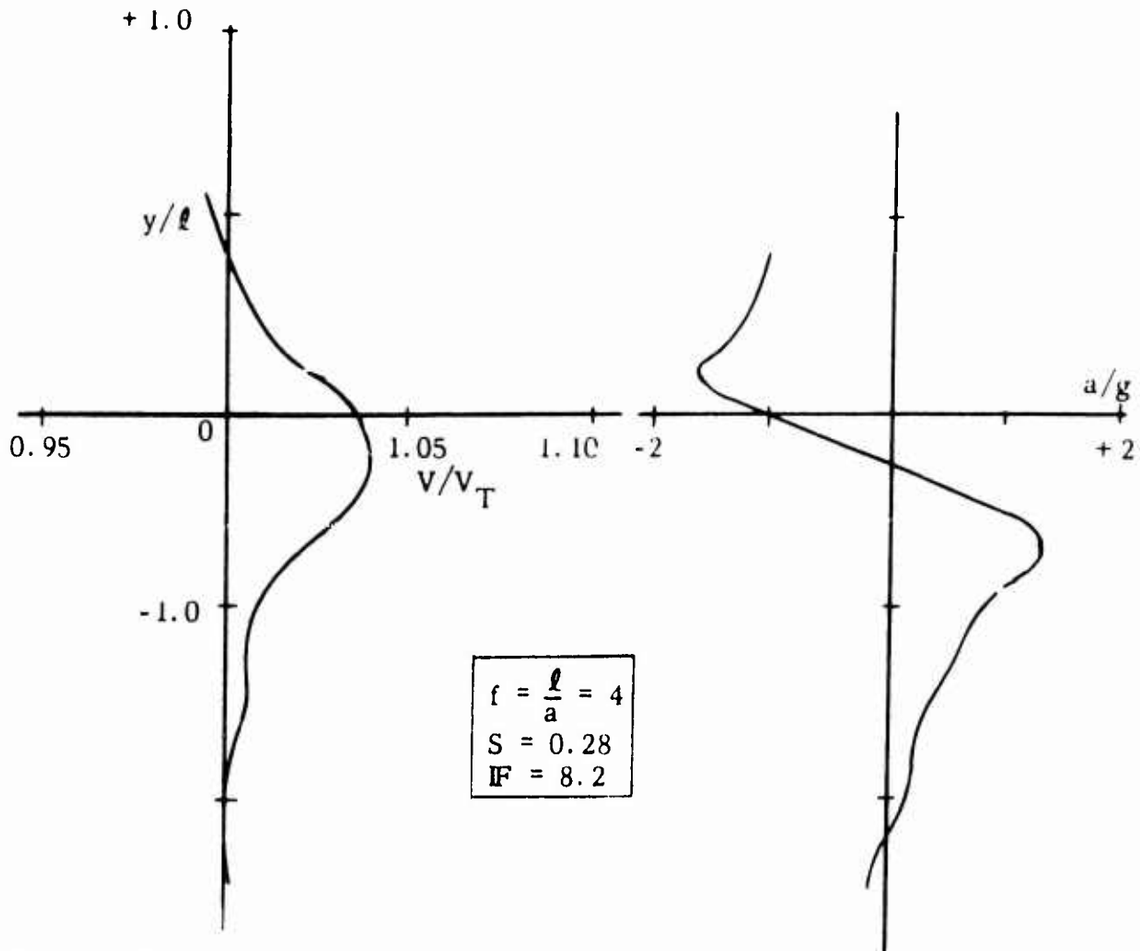

Fig. 3. Typical Experimental Velocity and Acceleration Profiles.

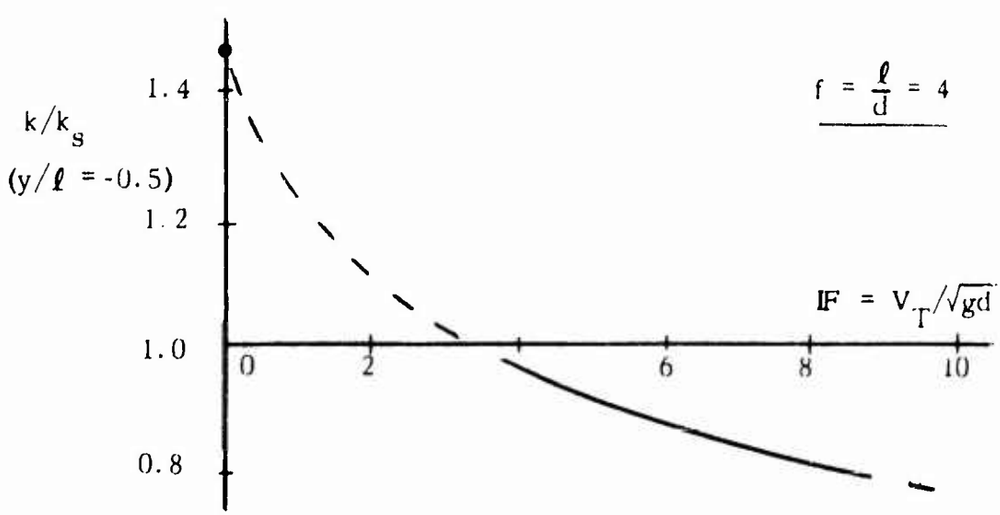

Fig. 4. Experimentally Observed Froude Number Variation in Added Mass Coefficient

Furthermore, this approach says nothing about the entrained water which appears to be a significant feature of the occurrences. This report, then, summarizes calculations of intermediate validity which give some indication of the relative importance of the various factors, even though treating certain ones rather crudely.

Certain problems are indicated as being important and will be considered in the following sections of this report. They are the approach of a buoyant body to its terminal velocity, the variation in added mass, buoyancy and drag as the body passes through the interface, and the entrainment of water with the exiting body.

I 6. Acknowledgements

The work reported is hardly the result of the solitary work of the author. Thus his colleague, M. E. Clark gave valuable advice concerning some of the integrals of Chapter III and in general concerning other phases of the work. The experimental results referred to at various points were obtained with Professor Clark (1). The series calculations of Chapter III were made by A. E. van Maele and J. C. F. Chow as student assistants. As part of his work as Research Assistant on the project Yau Wu collaborated with the author in the added mass analysis of Chapter IV as well as making some of the calculations of rise distance (Chapter III). The displacement volume calculations of Chapter VI were initiated by J. Chow as part of his work as Research Assistant.

$$D = C_w \frac{\rho}{2} A_w V^2 \tag{3}$$

where A_w represents the wetted or surface area of the body. On this basis Millikan's laminar boundary-layer analysis* leads to a coefficient, for a body of fineness ratio (ℓ/d) of 8.16, given by the relation

$$C_w = \frac{1.67}{\mathbb{R}_\ell^{1/2}} \tag{4}$$

where the Reynolds number $\mathbb{R}_\ell$ is based on the length of the body. This represents only the skin-friction contribution to the drag. Millikan noted that separation did not occur for streamlined bodies and assumed that this drag thus represented the total drag. For comparison, the flat-plate relation for this coefficient** is given by

$$C_w = \frac{1.328}{\mathbb{R}_\ell^{1/2}} \tag{5}$$

For the turbulent boundary layer the coefficient according to Millikan's 1/7th power law calculation of the 8.16 fineness body is

$$C_w = \frac{0.077}{\mathbb{R}_\ell^{1/5}} \tag{6}$$

---

* Millikan calculated the variation in drag for an airship model, termed the NPL long model, which had been tested in many tunnels (cf. Dryden and Kuethe). His results are presented in terms of a coefficient based on an area represented by the volume of the model to the two-thirds power. Dryden and Kuethe (8) give the linear dimensions as well as the length, diameter, and volume. Difficulty was experienced by the author in ascertaining the surface area of this model. Different methods of estimating the area did not agree. The more accurate method lead to a value of about 1.6 for the constant in Eq. 4. A less accurate method lead to a value of 1.69. Study of the material presented by Goldstein (10, p. 517) suggests that 1.67 is about the proper value. Considerable attention has been devoted to the results of Millikan's analysis of an f = 8.16 body in this section, since this represents about the only complete drag calculation available for a body of about the proportions of interest. The results lie between the well-known flat-plate drag results and the completely-empirical results being considered.

** For an ellipsoid of fineness ratio 4, the friction calculations of Chapter V yield a constant of 1.44 for the frictional portions of the drag. This, however is estimated to be only 45 percent of the drag, the rest being pressure drag from separation.

The comparable flat-plate result has the constant of 0.074. A more appropriate relation for the turbulent flat-plate skin friction is the Prandtl (1932) interpolation formula

$$C_w = \frac{0.455}{(\log R_\ell)^{2.58}} \qquad (7)$$

More recent expressions for the flat plate drag coefficient by Coles (1954) and Landweber (1953) are slightly below Eq. 7 at Reynolds numbers below 10^9.

In estimating the drag of a fine body at the Reynolds numbers of the order of interest here, the major question is that of the critical Reynolds number for transition from laminar to turbulent flow. Flat-plate data on this transition indicates that it will occur at Reynolds numbers from 10^5 to 3×10^6 or larger. Assuming that body curvature has little effect, a reasonable value to take for calculation is 10^6. Hoerner in converting the available data on the drag of fine bodies to the C_w type coefficient also adjusted the data (by the turbulence-factor method) to correspond to that for this same critical Reynolds number. The question of pressure-drag contributions depending upon the streamlining of the body's tail is important. The ellipsoids of interest do not have the streamlined tails of the bodies considered by Hoerner and Millikan.

The most probable variation in the coefficient C_w with Reynolds number and fineness ratio based on the above considerations is presented in Fig. 5. This figure is based on Hoerner's Fig. 5.11 (13), with a few minor changes. The appropriate flat plate relations, Eqs. 5 and 7, are shown together with a transition curve between them for the mixed flow occurring with a transition Reynolds number of 10^6. This curve has been calculated according to Prandtl's mixed flow approach. Also shown on the plot is Eq. 4 for the 8.16 fineness-ratio body of Millikan. This relation has led to the increase in the coefficients for the finer bodies over the values suggested by Hoerner. Otherwise, Fig. 4 follows his estimated curves rather closely. As an independent check on these estimates one experimental point is shown, as determined from Jones (14) measurement of the drag of fineness-ratio 4 ellipsoid. The agreement within a few percent is good and suggests that a reasonable allowance has been made for separation from the blunt tailed ellipsoids.

II.3. Terminal Velocities of Bare Models

When the buoyancy-propelled bodies reach terminal velocity they are in equilibrium and the buoyant force B is balanced by the weight W and the drag D_T at terminal in an unlimited fluid. Thus

II TERMINAL VELOCITY OF SMALL BUOYANT BODIES

Since it is desirable to perform the experimental studies of water exit with bodies approaching the free surface at a constant velocity, it was necessary to know what terminal velocities to expect. One method of achieving this consideration would be through experiment; however estimates made of the rise distance required to reach near-terminal velocities indicate that distances of five to twenty-some feet would be required for the bodies of interest. These distances are not easily available and the test bodies were not always stable over such lengths of travel. Therefore, it has been necessary to calculate the probable terminal velocities from drag information.

The drag of bodies results from skin-friction and normal-pressure distributions on the surface. These depend greatly upon the nature of the flow, i.e., the boundary-layer development along the body surface. Since the boundary layer about these bodies is apt to be partly turbulent, and transition conditions are not too clear even in simple flow cases, unequivocal results are not possible either experimentally or analytically. Following a consideration of the skin friction for elongated bodies the available drag-coefficient indications are evaluated to permit estimates for the ellipsoidal bodies of interest. This permits calculation of the expected velocities, as a function of body size, fineness and specific gravity. The few experimental results, which it has been possible to obtain, are also presented for comparison with the predictions.

II 1. Skin Friction of Fine Bodies

It has been stated by many authorities that the resistance or drag of a streamlined body is almost entirely due to skin friction (cf. (6), p. 15 or (8), p. 14). Since the bodies of basic concern in this study are rather fine ($\ell/d > 4$) it was thought at first that the resistance and hence terminal velocity could be calculated by using well established flat-plate skin-friction relations and that the only question would be the Reynolds number value for transition from laminar to turbulent flow in the boundary layer. There was a possibility that a small additional term might be needed to allow for separation of the flow near the tail of the body. Calculations of the terminal rise velocities under the above assumptions were made, but the subsequent more rational, but less precise, calculations have indicated that the velocities obtained were of the order of 40 percent too high for laminar flow and about 10 percent too high for a mixed laminar-turbulent boundary-layer flow.

A much more exact approach to determination of the body drag would be through the calculation of the boundary-layer growth along the curved surface of the body. The first such calculations were by Millikan (7) in 1932, although an earlier "equivalent flat plate" (but with a varying velocity outside of the layer) calculation was made by Dryden and Kuethe (8). Millikan used the Karman momentum-integral method for determining the rate of growth of the laminar boundary layer with the velocity distribution approximated by a parabolic profile* Since Millikan used the 1/7th power-law velocity distribution for the turbulent portions of the boundary layer. Moore (9) in 1935 presented an analysis in terms of von Karman's newly developed logarithmic law for the velocity profile. This lead to a significant increase in the drag coefficient at the higher Reynolds numbers. Further discussion of this type of calculation and comparison of the predictions with wind tunnel measurements on various airship hulls is presented in Goldstein (10).

The methods of drag calculation discussed above are still rather approximate. Analysis methods for boundary-layer flows have been considerably advanced in recent years. The 1954 paper by Weighardt (11) presents a simple method for analysis of the laminar layer which appears more neatly correct and the situation in regard to the turbulent layer is well summarized by Granville (12). Suitable estimation for the drags of the test models for the present study probably should be made through such boundary-layer calculations (cf. calculations of Chapter V). However, these are rather lengthy and are still approximate due to necessary assumptions about the transition Reynolds number and behavior of the separated flow at the tail of the body. The approach is therefore made via empirical consideration of drag-coefficient results.

II. 2. Drag Coefficient Information

The drags and terminal velocities of the test bodies have been estimated with the aid of Hoerner's analysis (13) of the available drag-coefficient data. Hoerner, however, has transferred the results into a skin-friction type of coefficient. This permits one to compare directly with the flat-plate skin-friction predictions. The drag is therefore represented by the relation

---

* More up to date laminar boundary-layer calculations based on more refined velocity profiles are possible following the work of Pretsch (17), as utilized in Chapter V.

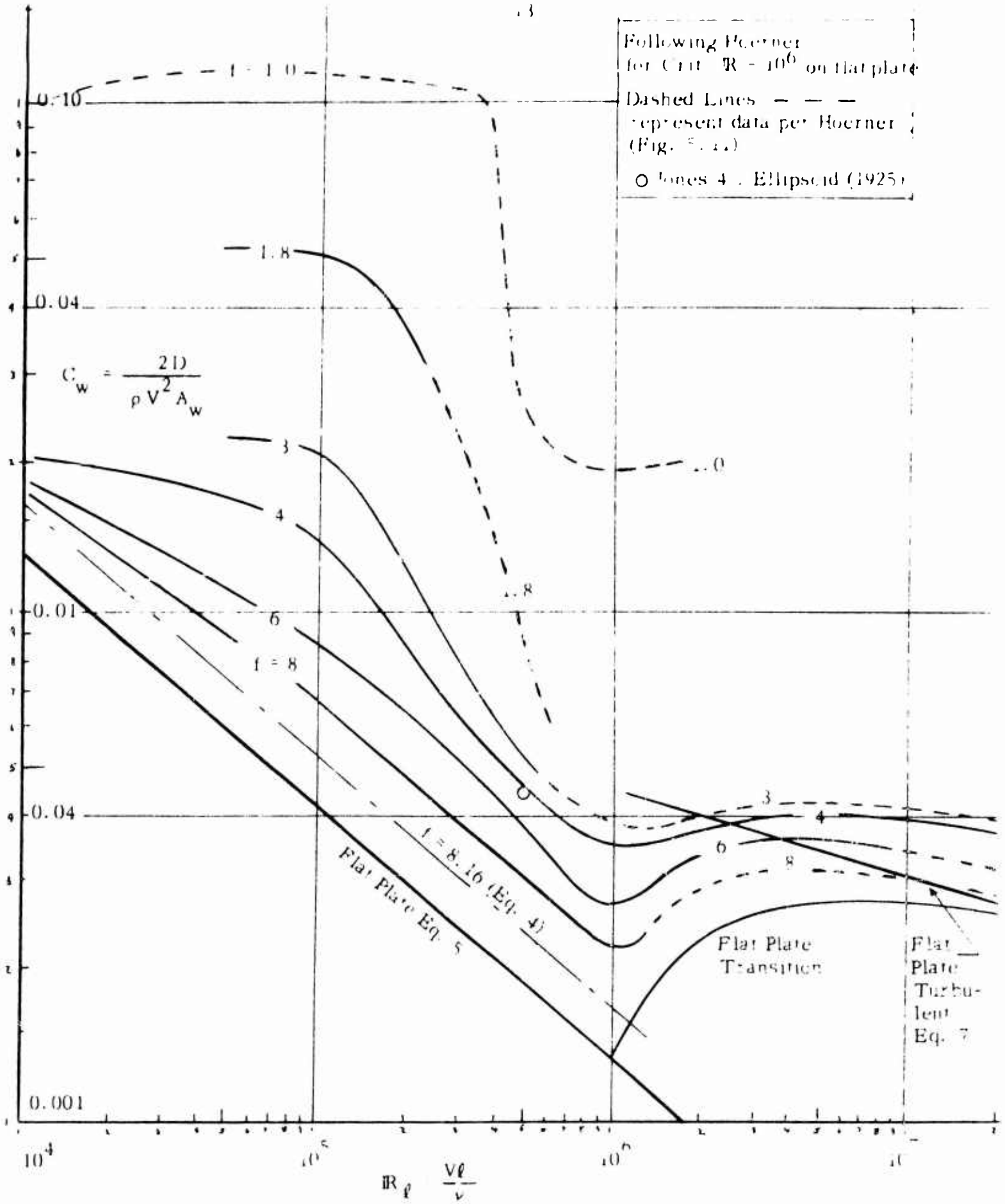

Fig. 5. Surface Drag Coefficients for Axisymmetric Bodies

$$B - W = \forall \gamma (1 - S) = D_T \qquad (8)$$

where $\forall$ represents the volume and S the specific gravity of the body, while γ is the specific weight of the fluid (water)

For the bare, i e unfinned, test bodies the drag D_T in Eq 8 is calculated with Eq 3 and C_w evaluated from Fig 5. This has been done for the one- and two-inch diameter test bodies (ellipsoids of revolution) of fineness ratio of 4 and 8 The calculation procedures are presented in a later section The terminal velocities thus predicted for the bare models are indicated in Fig 6a In some cases two possible terminal velocities are shown, one for the model with transition from laminar to turbulent flow in the boundary layer at about 10^6, as indicated in Fig 5, and the other assuming the laminar flow continues along the model with no transition The C_w values in the second case were obtained by extending the laminar lines in Fig. 5 parallel to the flat-plate line. For the blunter body ($\ell/d = 4$) this may be a poor assumption

The possibility of lower critical Reynolds numbers was also considered. Assuming a flat-plate transition Reynolds number of 5×10^5 and that at high Reynolds numbers (say 3×10^7) the values of C_w are the same as shown in Fig 5, suitable transition curves were faired in on a similar plot (cf. the upper plot of Fig 7) In this case terminal velocities were calculated only for the finned bodies.

II 4 Terminal Velocities of Finned Models

Since the test models are unstable as they rise through the water (1), it has been necessary to add stabilizing fins at the tail. The surface area of these fins is not negligible, hence the terminal velocities just presented are too high. An attempt was therefore made to estimate the additional drag resulting from the fins

The fins are low-aspect-ratio flat plates Since they are thin their drag is calculated as though they were flat plates Since these are one fifth to a tenth as long as the model, the boundary layer on them should remain laminar and Eq. 5 has been used to calculate the additional drag D_f due to the fins. The total drag is now $D = D_b + D_f$ where D_b represents the bare model drag as previously estimated In terms of the drag coefficient (cf. Eq. 3) this can be expressed as

$$C_w = C_{wb} + \frac{8A_f}{A_w} C_F \qquad (9)$$

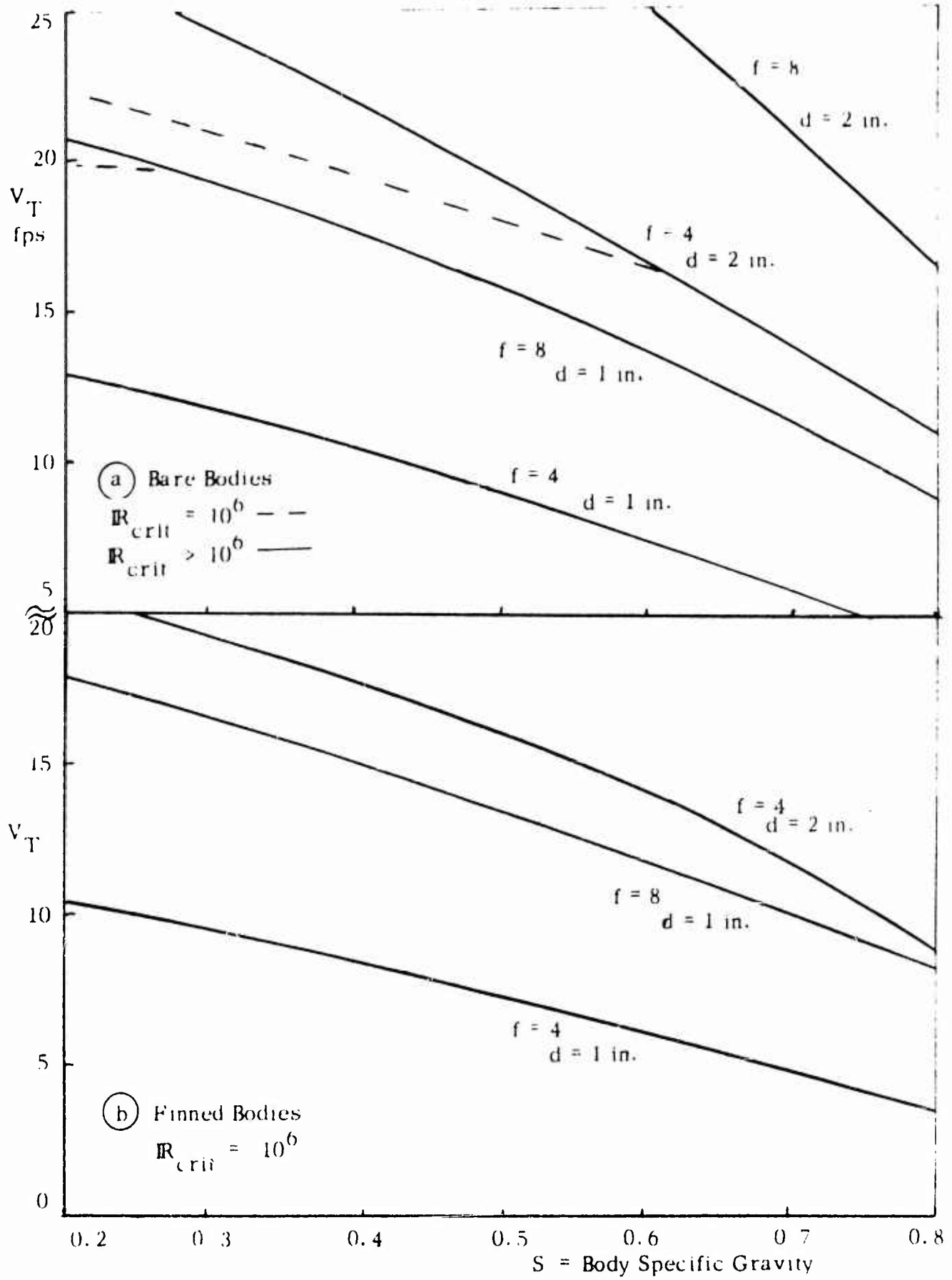

Fig. 6. Calculated Terminal Velocities of Ellipsoidal Bodies in Water.

where the first term is the bare model value given by Fig 5 and the second term is the increment due to the fin. Here A_f is the surface area of one side of a fin* and C_F is the mean flat plate friction coefficient at the fin-length Reynolds number. A simple version of this equation that indicates more directly the relative contribution of the fins is

$$C_w = C_{wb}\left(1 + \frac{8A_f}{A_w}\,\frac{C_F}{C_{wb}}\right) \qquad (9a)$$

For the range of bodies and Reynolds numbers of interest, the fin contribution to the drag is 17 to 31 percent of the bare model drag. This leads to a 7 to 12 percent decrease in terminal velocity.

Corrected values of C_w in accordance with Eq. 9a have been calculated for ℓ/d equal to 4 and 8 bodies similar to the test models. These calculations are based on the constants $8A_f/A_w$ of 0.25 for the $\ell/d = 4$ body and 0.13 for the $\ell/d = 8$ body with fin lengths (for Reynolds number calculations) of 0.16 and 0.08 of the model lengths. The values of C_w thus obtained are indicated in Fig. 7 for transition Reynolds number of 5×10^5 and 10^6. It should be noted that in accord with Eq. 9, the drag coefficient C_w is to be used with the body surface area.

The terminal velocity of several bodies similar to the test models have been calculated using C_w from Fig. 7. The results are indicated in Fig. 6b as a plotting of terminal velocity V_T versus specific gravity S for bodies of two fineness ratios and two diameters. The range of velocities of interest is seen to be from 5 to 20 fps for the 1- and 2- inch bodies.

II.5. Method of Velocity Calculation

Initially the terminal velocities were calculated by trial and error processes for given body shape, size and specific gravity. The results were then checked by the quicker indirect method starting with the velocity and solving for the specific gravity. The results were also checked by another direct method based on fitting portions of the C_w vs. R_ℓ curves with power-law equations** such that $D = KV^n$. Such relations

---

* The factor 8 thus appears since there are four fins with two sides each.

** Such laws are used in exterior ballistics and are named after the Russian Mayevski, who found them appropriate for projectiles with various values of K and n in different velocity zones.

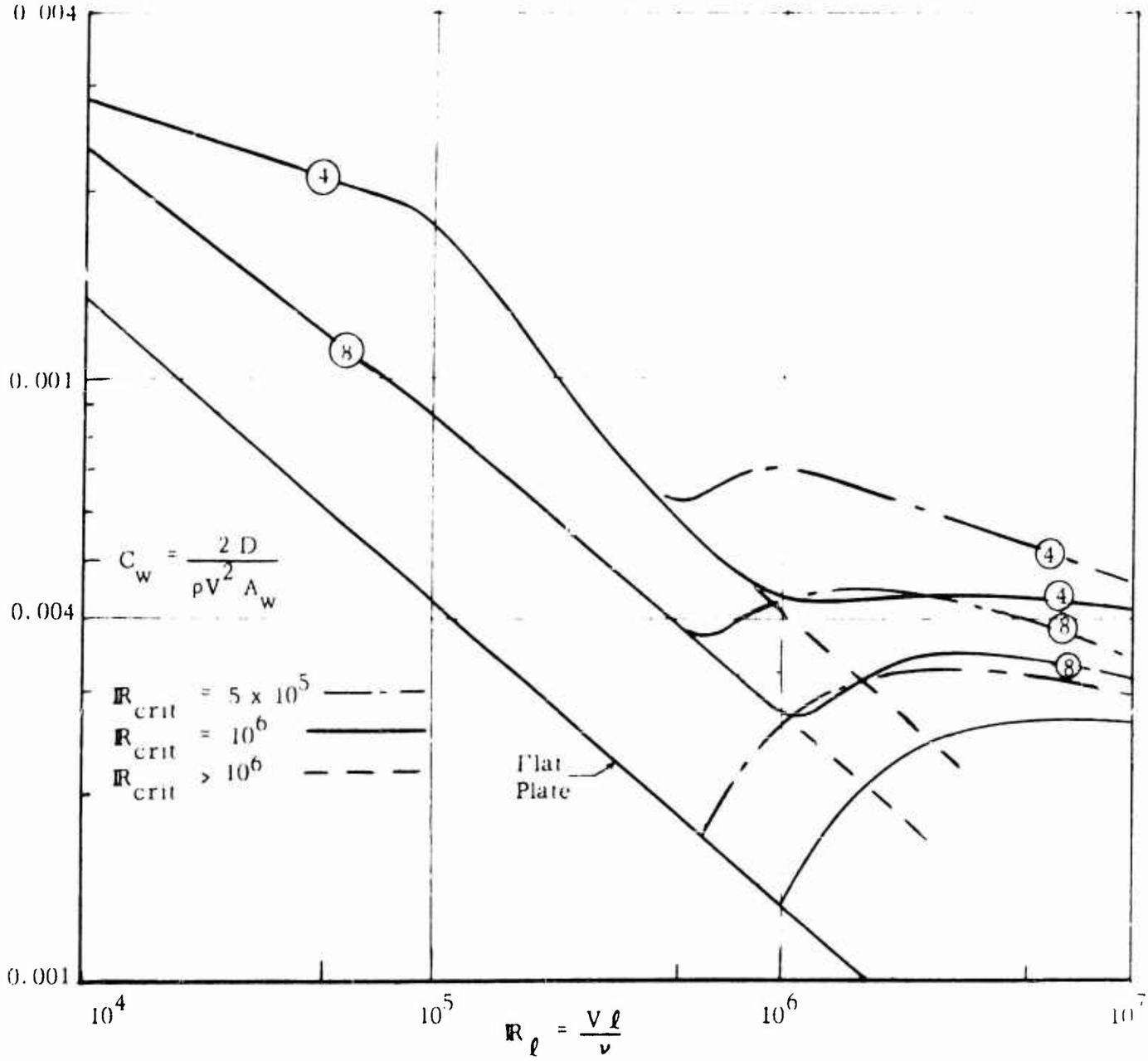

Fig. 7. Drag Coefficients of Finned Bodies

are discussed in Chapter III. This represents the simplest calculation method once these power-law relations have been determined. Since the calculations were completed a quick trial and error method, working directly from the C_w vs $\mathbb{R}_\ell$ plots, has been developed. This last method also permits one to visualize the effect of various factors on terminal velocity and hence will be indicated briefly.

For the terminal situation Eqs. 3 and 8 are equated, whence

$$C_w \frac{V^2}{2} A_w = (1 - S) g \forall$$

In terms of the relations between A_w and $\forall$ and the body length and diameter, the following relations may be introduced for ellipsoids

$$\forall = \frac{\pi}{6} d^2 \ell = v \ell^3 \quad ; \quad v = \frac{\pi}{6} \left(\frac{d}{\ell}\right)^2$$

$$A_w = a \ell d \quad ; \quad a \cong 2.5 \qquad \text{(cf. Fig. A1)}$$

The preceeding equation now may be written

$$C_w = \frac{a}{2v} V^2 = (1 - S) g d f^2$$

where $f = \ell/d$ = fineness ratio. Solving for the velocity, this yields the relation

$$V = \sqrt{g d} \sqrt{\frac{2f^2 v}{a}} \sqrt{\frac{1 - S}{C_w}} = \mathbb{K} \sqrt{gd} \sqrt{\frac{1 - S}{C_w}} \qquad (10)$$

For ellipsoids

$$\mathbb{K} = \sqrt{\frac{2 f^2 v}{a}} = \sqrt{\frac{\pi}{3a}} \cong 0.647$$

This factor is nearly a constant ($\pm$ 1/2 percent) since a varies little with f. Thus the terminal velocity is

$$V_T = 0.647 \sqrt{gd} \sqrt{\frac{1 - S}{C_w}} \qquad (10a)$$

and the Froude number at terminal is

$$\mathbb{F} = V_T / \sqrt{gd} = 0.647 \sqrt{(1 - S)/C_w} \qquad (10b)$$

These suggest an independence from body fineness ratio, but of course, C_w is a function of f as well as $\mathbb{R}_\ell$.

Calculation of terminal velocity, for given f and S, now proceeds quickly. The drag coefficient is initially estimated from Fig. 5 or 7 and a V_T value found from Eq. 10a. This permits calculation of $\mathbb{R}_\ell$ and a new estimate of C_w. The result converges rapidly.

II.6. Experimental Verification

After several years of testing and the introduction of an air gun, to get the bodies up to speed faster, a modicum of experimental information has been obtained on the terminal velocities of the 1- to 4- in. diameter test bodies. The results obtained with the gun assisting the bodies up to speed are felt to be more definitive since velocities above, as well as below, terminal can be obtained.

Some of the apparent terminal velocities found experimentally for the several test bodies were presented in an earlier report (1). Based on the specific gravity and size of the body the calculated terminal velocities were found and compared. This comparison, together with a few additional values for the larger bodies is summarized in graphical form in Fig. 8. In three cases, where the calculated terminal velocity was more than five percent greater than the observed, the calculation has also

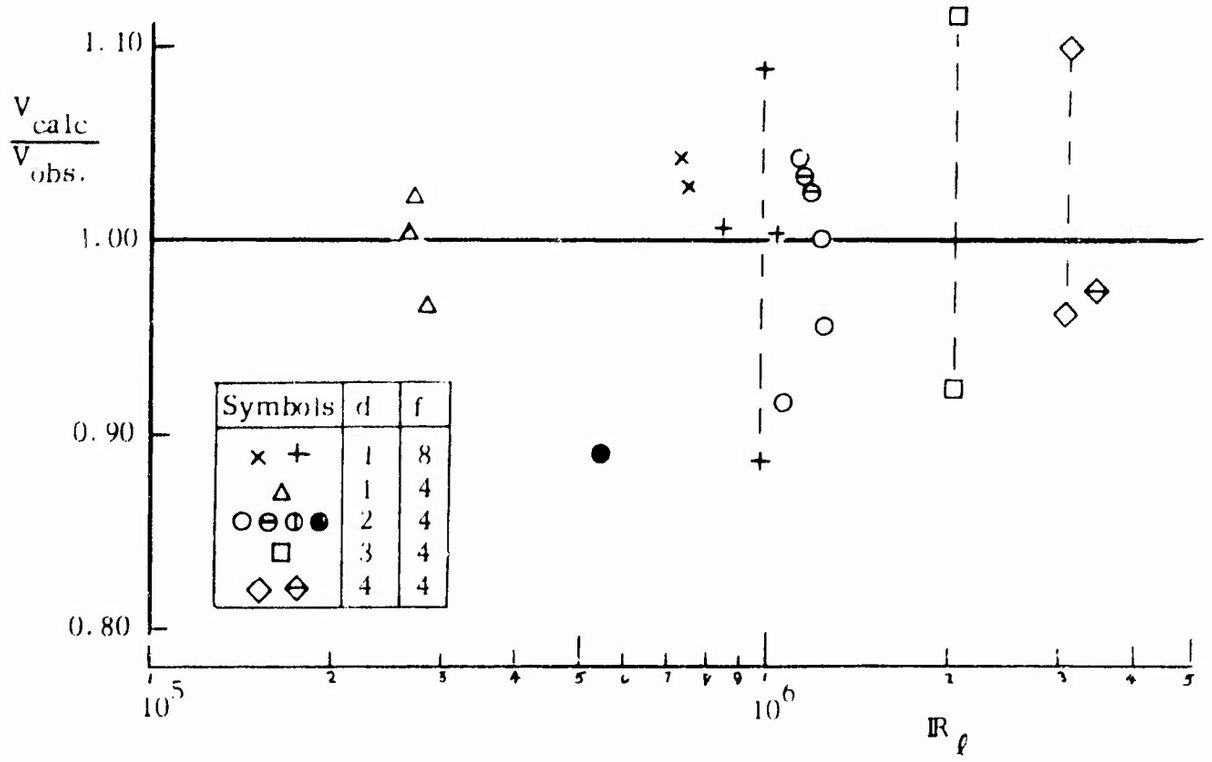

Fig. 8. Experimental Verification of Calculated Terminal Velocities

been made on the basis of a critical Reynolds number of 5×10^5. This leads to a bracketing of the observed results as indicated by the vertical dashed lines. Apparently transition occurred between 5×10^5 and 10^6. In the case of the highest Reynolds number test with the 4-in. diameter body, the water in the test tank was allowed to rest at least a half hour before the body was "shot". This settling period seems to have permitted a higher transitional Reynolds number to be reached, close to the 10^6 value assumed for the majority of the calculations. Only two cases of the calculated velocities being more than five percent below the observed, or vice versa, are shown. There is no explanation for the large divergences in these cases. Due to the difficulty of assessing exact achievement of terminal velocity in the experiments, the occurrence of most of the data within a tolerance of plus or minus five percent must be regarded as a good check.

Another way of verifying the approach used in the calculation of terminal velocity is by calculating C_w from the observed V_T results. From Eq. 10b the

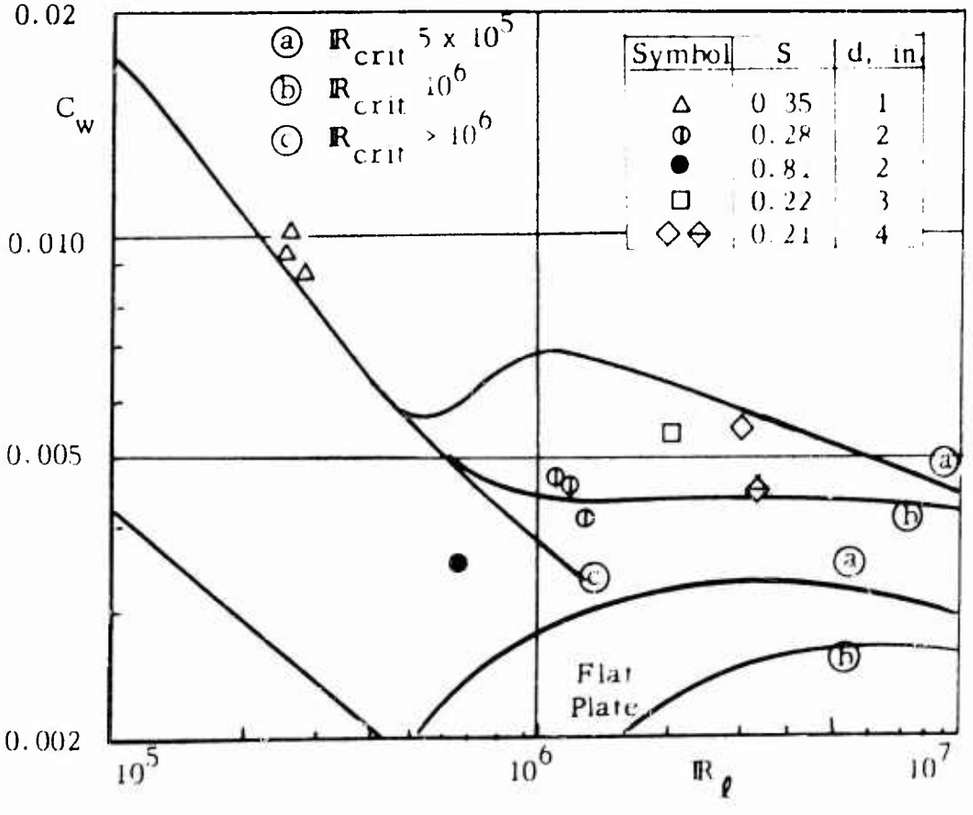

Fig. 9. Drag Coefficients Evaluated from Terminal Velocities Compared with Predictions. (Finned Ellipsoids of f = 4)

drag coefficient in terms of the physical conditions of the test is

$$C_W = 0.418 \frac{1 - S}{\mathbb{F}_T^2} = 0.418 \frac{(1 - S)gd}{V_T^2}$$

The experimental terminal velocity data on the $\ell = 4$ bodies has thus been reduced to C_W values. These are shown in Fig. 9 in comparison with the curves of Fig. 6; except for the 2-in. body with S of 0.81, the agreement is very good. Early transition (at perhaps $\mathbb{R}_\ell = 7 \times 10^5$) is apparent for some of the tests with the 3- and 4-in. bodies. Results corresponding to transition at a higher Reynolds number ($\sim 10^6$) are seen to have been achieved by waiting for disturbances in the water to decay.

Although less data has been obtained with the finer body ($\ell = 8$), agreement comparable to that shown in Fig. 9 has been obtained.

II.7 Size Effect on Velocity and Froude Number

In numerous hydrobalistics situations it is desirable to know how the terminal velocity of a buoyant body varies with its size. For the present problem it was desirable to study water-exit phenomena over the widest possible range in Froude number and (in fact) the interrelationships between d, V_T and $\mathbb{F}_T$ were considered briefly earlier (1). The effects of diameter on V_T and $\mathbb{F}_T$ are simply evaluated from Fig. 7 with the aid of Eqs. 10a and 10b. It seems appropriate to note just what should occur as d is increased*.

For a body of given shape ($\ell = \ell/d$, and specific gravity Eq. 10a and 10b show that

$$V_T \sim \sqrt{d/C_W}$$

$$\mathbb{F}_T \sim 1/\sqrt{C_W}$$

* The significance of these considerations becomes apparent when it is noted that the tests of the 3- and 4-in. diameter bodies were initiated in the hope that Froude numbers higher than those obtained with the 2-in. body could be obtained. Since in going from the 1- to 2-in. size the Froude number increased in the ratio 1.6; it was hoped that further size increase would achieve some further increase in $\mathbb{F}$. Actually there was negligible gain with the 3-in. body and about a 10 percent gain with the 4-in. As will be noted these limited increases are predictable.

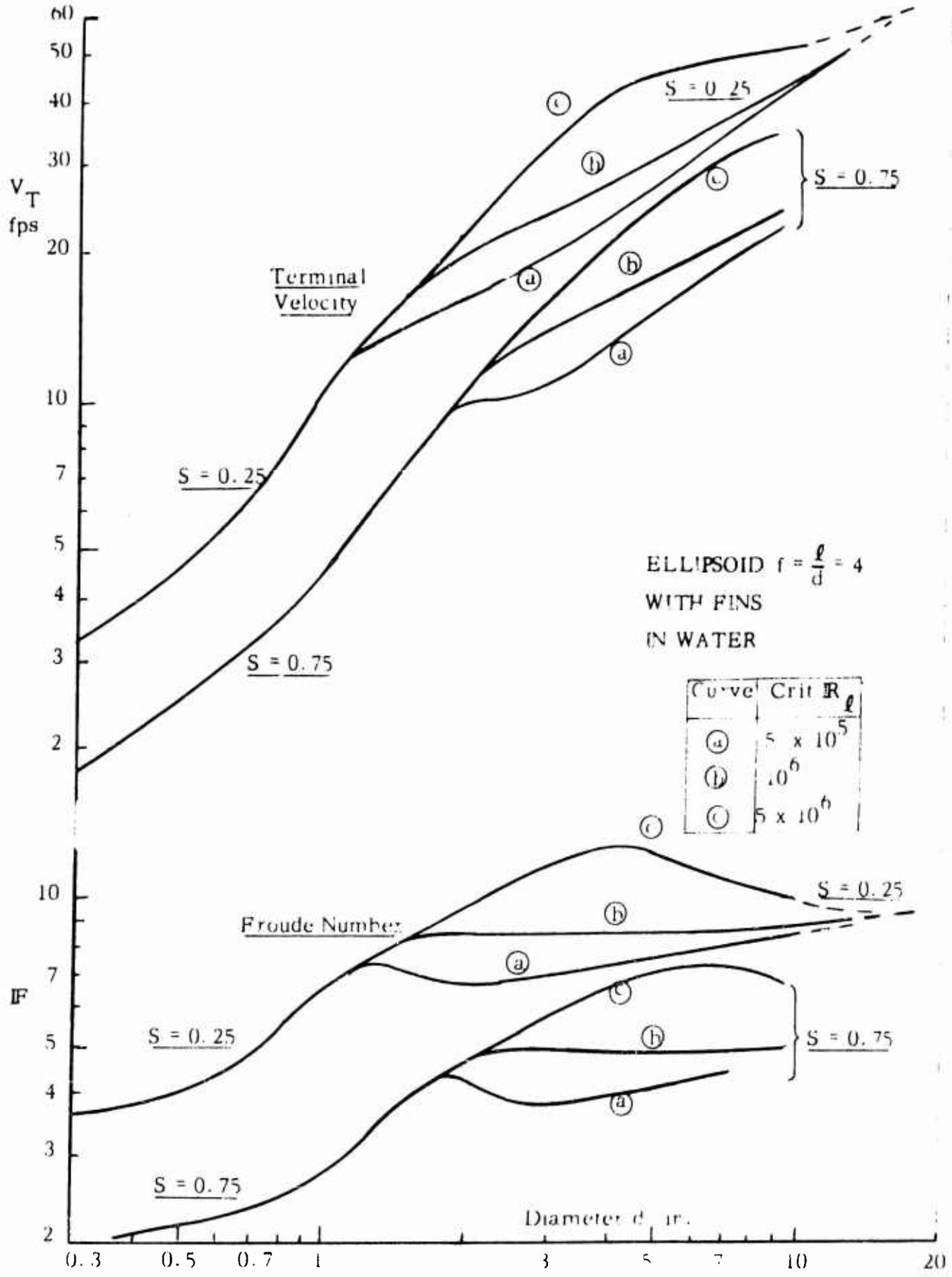

Fig. 10. Variation in Velocity and Froude Number with Diameter.

Thus from Fig 5 or 7 for the f = 4 body, F_T should be nearly constant in the R_f range 10^6 to 10^7 This is the range covered by the light 2-in , 3-in and 4-in. bodies in the water exit tests. They all achieved F_T values in the range 8 to 9 In this range V_T is, of course, proportional to the square root of the diameter.

As a more explicit indication of the size effect, calculations of V_T and F_T have been made for the f = 4 body at two specific gravities over a considerable range in sizes The results are presented in Fig 10. It is apparent that the only way to vary the Froude number at diameters above 2 inches is via changes in body density or via delay in transition (increase in transition Reynolds number R_c). For sizes up to 1 5 in the velocity increases roughly linearly with diameter; above this size it varies roughly as the 5/3 power of the size The use of sand-grain boundary-layer transition devices to initiate premature turbulent flow and hence produce lower terminal velocities on given bodies is discussed in another report from this project (15).

For diameters above about one foot, a different power applies but the calculations have not been carried far enough into the turbulent boundary-layer region to define this Possible effects due to variation in transition Reynolds number are seen to be appreciable for body sizes between 2 and 10 inches.

III THE RISE DISTANCE--A BALLISTIC PROBLEM

It is obvious that the experimental studies of the water-exit behavior of buoyancy-propelled bodies should be conducted after the body has risen sufficient distance to reach terminal velocity (1). Since there seemed to be no available information on the determination of the required rise distance to reach terminal, it has been necessary to develop a method of analysis to be used in making such predictions. This problem in external ballistics has been solved on the conventional assumption that the drag at any velocity is independent of the acceleration of the body. The effect of this assumption and that of negligible rate of change of the added mass of the body is thought to be small. It has also been assumed that the rising bodies are stable in their motion

III. 1. Basic Theory

To predict the distance required for a buoyancy-propelled body to reach terminal velocity, the relation between distance and velocity of the rising body is needed. This is obtained from a relation for the acceleration due to the forces acting on the body in the unsteady motion. As sketched in Fig. 1, the rising body is subjected to three forces, buoyancy pulling upward and weight and drag downward*. Until terminal velocity is reached the buoyant force is the larger and the body is accelerated upward. Applying Newton's second law of motion to the body,

$$B - W - D = \frac{W}{g} a = \frac{W}{g} \frac{dV}{dt} \tag{11}$$

The first two forces are simply expressed in terms of the volume and specific gravity S, hence

$$\gamma (1 - S) \Psi - D = \gamma \frac{S}{g} \frac{dV}{dt}$$

where γ is the specific weight of the fluid medium, in this case water. It is assumed that the drag D is uniquely associated with the velocity of the body through the water and is independent of acceleration. Therefore, a simple Mayevski-type resistance law is chosen,

$$D = K V^n \tag{12}$$

---

* In these calculations the body is assumed sufficiently far from free or rigid surfaces so that the forces which appear there are negligible.

and at terminal velocity V_T, the acceleration is zero whence

$$(B - W) = D_T = K V_T^n \tag{12a}$$

Inserting these expressions into Eq. 11 one obtains the relation

$$K (V_T^n - V^n) = \gamma \frac{S\forall}{g} \frac{dV}{dt}$$

or

$$1 - (V/V_T)^n = \frac{S}{g(1 - S)} \frac{dV}{dt} = \frac{\beta}{g} \frac{dV}{dt} \tag{13}$$

where $\beta = S/(1 - S)$. This yields a simple relation between velocity and time.

Before proceeding with the determination of the relation between velocity and distance one additional factor should be added -- the effect of added mass. This added mass must also be accelerated and it is assumed that the rate of change of this added mass is a second order effect. The right side of Eq. 13 must be multiplied by the factor

$$a = 1 + \frac{k_s}{S} \tag{14}$$

where the subscript s refers to the submerged or infinite fluid value of k. Eq. 13 becomes

$$1 - (\frac{V}{V_T})^n = \frac{\beta a}{g} \frac{dV}{dt} \tag{13a}$$

An expression for the distance y from the start of the rise is obtained by noting that $V = dy/dt$, hence from Eq 13a

$$\frac{dy}{V} = dt = \frac{\beta a}{g} \frac{dV}{1 - (\frac{V}{V_T})^n}$$

If the ratio V/V_T is expressed as the variable x, this becomes

$$dy = \frac{\beta a V_T^2}{g} \frac{x\,dx}{1 - x^n} \tag{15}$$

The integral expression for the rise distance y to a point where the velocity is x times the terminal velocity ($x < 1$) is thus

$$Y = \frac{y g}{\beta a V_T^2} = \int_0^x \frac{x\,dx}{1 - x^n} \qquad (15a)$$

The rise distance is seen to vary with the square of the terminal velocity.

III. 2 Solution of Rise Distance Equation

Evaluation of the integral in Eq. 15a in closed form is possible for n values of 1, 2, and 3. The constant of integration is evaluated from the condition $y = 0$ for $x = 0$, and the following results are obtained:

for $n = 1$

$$Y = -x - \log_e (1 - x) \qquad (16a)$$

for $n = 2$

$$Y = -\frac{1}{2} \log_e (1 - x^2) \qquad (16b)$$

for $n = 3$

$$Y = \frac{1}{3}\left[\frac{1}{2}\log_e\left(\frac{1 + x + x^2}{(x - 1)^2}\right) + \sqrt{3}\tan^{-1}\left(\frac{2x + 1}{-\sqrt{3}}\right) + \frac{\pi}{2\sqrt{3}}\right] \qquad (16c)$$

Of course, these all predict an infinite distance to reach terminal velocity $(x = 1)$. It is intuitively obvious that this should be so, since the approach to terminal velocity must be asymptotic as $(B - W)$ approaches D_T.

The exponent n actually varies from 1.3 to 2.5 depending on the Reynolds number range and fineness ratio of the body. By expanding the integrand of Eq. 15a in series form

$$\frac{x}{1 - x^n} = x + x^{n+1} + x^{2n+1} + x^{3n+1} + \ldots$$

and integrating, the solution becomes

$$Y = \frac{x^2}{r} + \frac{x^{n+2}}{n+2} = \frac{x^{3n+2}}{3n+2} + \ldots \frac{x^{pn+2}}{pn+2} \qquad (17)$$

Of course as x approaches unity the convergence of this series becomes very slow.

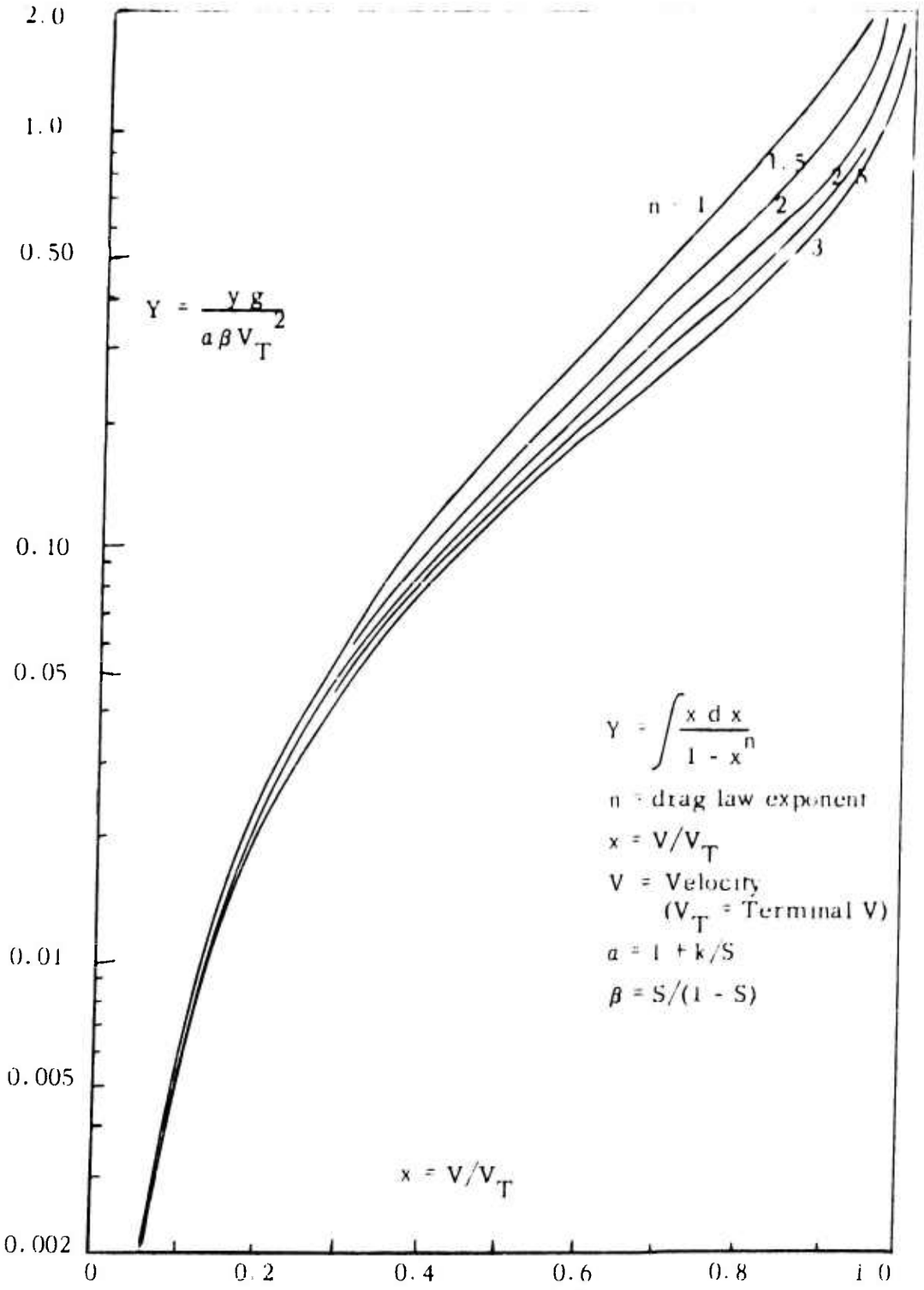

Fig. 11. Rise Distance Relations for Buoyant Bodies.

The series has been evaluated numerically for $n = 1.5$ and 2.5*. The results are indicated in Fig. 11 together with the solutions for $n = 1$, 2, and 3 from Eqs. 16.

The application of the solutions of Eq. 15a, as presented in Fig. 11 to the prediction of the rise distance is quite simple when n is a constant. Thus for a given n, this figure** gives one the value of the parameter $Y = yg/\beta a V_T^2$ required to reach a certain fraction x of terminal velocity. As $g/a\beta V_T^2$ is determinate, once the body and fluid are given, y can be directly calculated.

III. 3. Calculation of Rise Distance for n Variable

Unfortunately, as is apparent from Fig. 7, the drag coefficient for a body does not vary simply ($C_w = K\mathbb{R}^m$) with Reynolds number and the exponent m and hence n is therefore a variable. For a given body and fluid, n in Eq. 15 will have one value at low velocities and another at high velocities. The problem must therefore be solved in step-wise fashion, by making the elementary ballistic assumption that n is a constant over a certain range of velocities. Once this range is exceeded another value applies. With each range of n application, a different effective value of V_T applies.

The stepwise solution to the rise distance problem is best illustrated through an example. For clarity's sake a two step case will be illustrated. Thus, if only body skin friction entered, C_w would be given by the Blasius type relation for the laminar range and n would have the value 1.5. Transition to a turbulent boundary layer might be at a critical Reynolds number of 10^6. For a considerable range of velocities above the critical the exponent is then about 2.5. The body will rise in accord with the $n = 1.5$ curve with an effective or fictitious terminal velocity $V_{T\ell}$ which it would reach according to the laminar drag law if there were no transition to turbulence. When however, the velocity V_c corresponding to the critical Reynolds number is reached, the boundary layer will become partly turbulent. From this point on the $n = 2.5$ curve will apply for the rise, but with an effective origin y_e as though the body had been rising from the start with $n = 2.5$. Of course in this latter part of the rise the terminal velocity V_{Tm} to be used in the rise calculations is that for the (mixed flow) new drag law of $n = 2.5$. The general situation is depicted in Fig. 12.

---

* Numerical values obtained for the solution of Eqs. 16a, b, c, and 17 are presented in the Appendix (Section VIII. 5).

** For ease of calculation lines of constant x were plotted as Y vs. n. These plots are appended as Figs. A2 and A3 in Section VIII. 4.

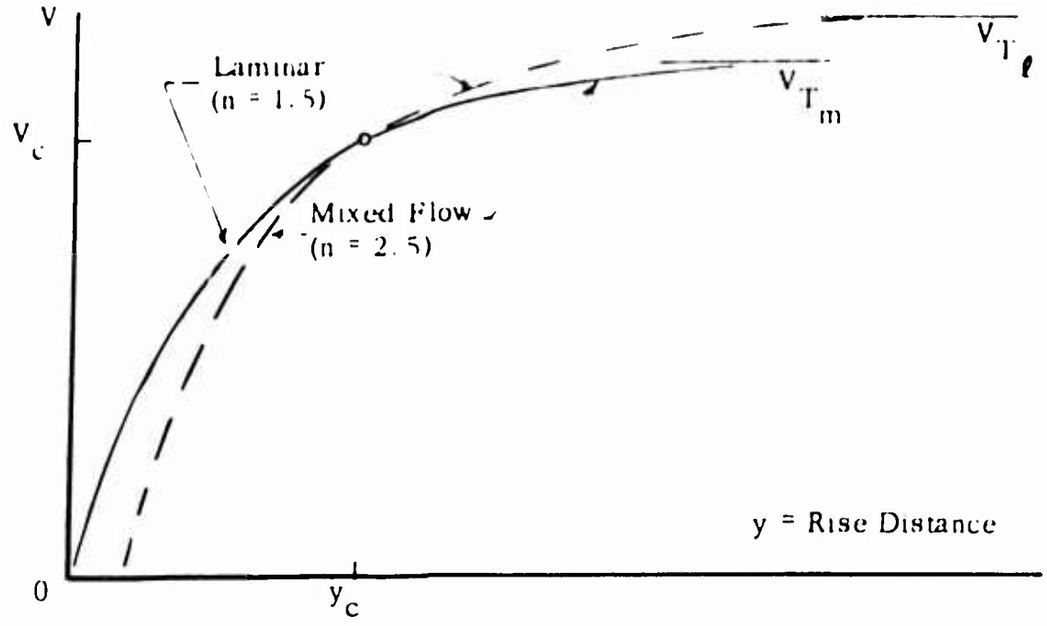

Fig. 12. Two Step Calculations of Velocity-Distance Relation for Buoyant Body

For simplicity of calculation the rise distance may thus be written for the final distance, with which one is really interested, as

$$y = y(x, n) = y(x, 2.5) - y(x_{c_{2.5}}, 2.5) + y(x_{1.5}, 1.5) \qquad (18)$$

The parenthetical terms are symbolic meaning that y is to be evaluated from Fig. 11 (or Figs. A2 and A3) for the particular value of $x = V/V_T$ and n. In the case of the critical point, x_c is different for the two exponents, even though the critical velocity is the same due to different terminal velocities applying. As may be seen from Fig. 12 the occurrence of mixed flow shortens the rise distance when n_2 is greater than n_1. This stepwise solution is obviously extendable to cases when more than two drag laws apply. For each step in which a separate value of n must be used, the calculation of the increment in y is based on the effective value of the terminal velocity for the particular drag law.

Study of the relation between the drag coefficient as a function of fineness ratio and Reynolds number (cf. Figs. 5 and 7) indicates that four or five drag laws are needed to cover the Reynolds number range of interest (about 10^4 to 10^7). For the various bodies of interest and (flat-plate) transition Reynolds numbers of 5×10^5 and 10^6, these have been evaluated and the several laws are tabulated in the Appendix (section VIII 3). All of the exponents are within the range of 1 to 3, for which the

unsteady motion equation (Eq. 15) has been solved. Since most of the rise distance occurs after the body has reached eight-tenths of the terminal velocity (cf. Fig. 12) a three step solution is adequate in most cases*, thus

$$y = y(x, n_3) - y(x_{c_{23}}, n_3) + y(x_{c_{22}}, n_2) - y(x_{c_{12}}, n_2) + y(x_{c_{11}}, n_1) \quad (18a)$$

where n_1 indicates the exponent for the first drag law, etc., $x_{c_{11}}$ indicates the critical velocity separating law 1 and 2 divided by the effective terminal velocity applicable to law 1 and $x_{c_{12}}$ indicates this same velocity divided by the effective terminal velocity for law 2. For x in the first term a value of 0.98 or so is chosen depending just how close to the terminal one desires to make the calculation.

III 4 Results for Typical Test Bodies

The rise distance as a function of the specific gravity of the body has been calculated for three typical test bodies, the 1-in. diameter finned model of $\ell/d = 4$, the 1-in. $\ell/d = 8$ finned model, and the 2-in $\ell/d = 4$ finned model (for $R_c = 5 \times 10^5$ and 10^6). The results are shown in Fig. 13. Except for the 1-in $\ell/d = 4$ body, where only 3 to 5 feet of rise distance is required, it is apparent that the necessary rise distance increases with increase in S and that 5 to 23 feet are needed. The rise distance also increases rapidly with length of the body and the transitional Reynolds number.

A few scraps of information on the rise distance are available from the experimental phases of this project (1). Thus over 4 feet were required for the 1-in $\ell/d = 8$ body ($S = 0.27$). In the case of the 2-in. $\ell/d = 4$ body about 6 feet were found to be necessary to reduce the acceleration to a small value. According to Fig. 13 some 7 to 9 feet should be required. In the case of the $\ell/d = 8$ body, 8 feet should be needed -- twice the four foot value noted to be insufficient. For a 1-in. $\ell/d = 4$ body it appeared that experimentally 3 to 4 feet were required to reach terminal velocity. This body had a specific gravity of about 0.33 whence Fig. 12 indicates a needed rise distance of 4 feet. Considering the experimental uncertainties involved in ascertaining when a body is close to terminal velocity, it would appear that a tolerable check on the calculations has been obtained.

---

* This is a fortunate exception to the usual ballistics problem in which the multiplicity of step-wise calculations makes such an approach inconvenient.

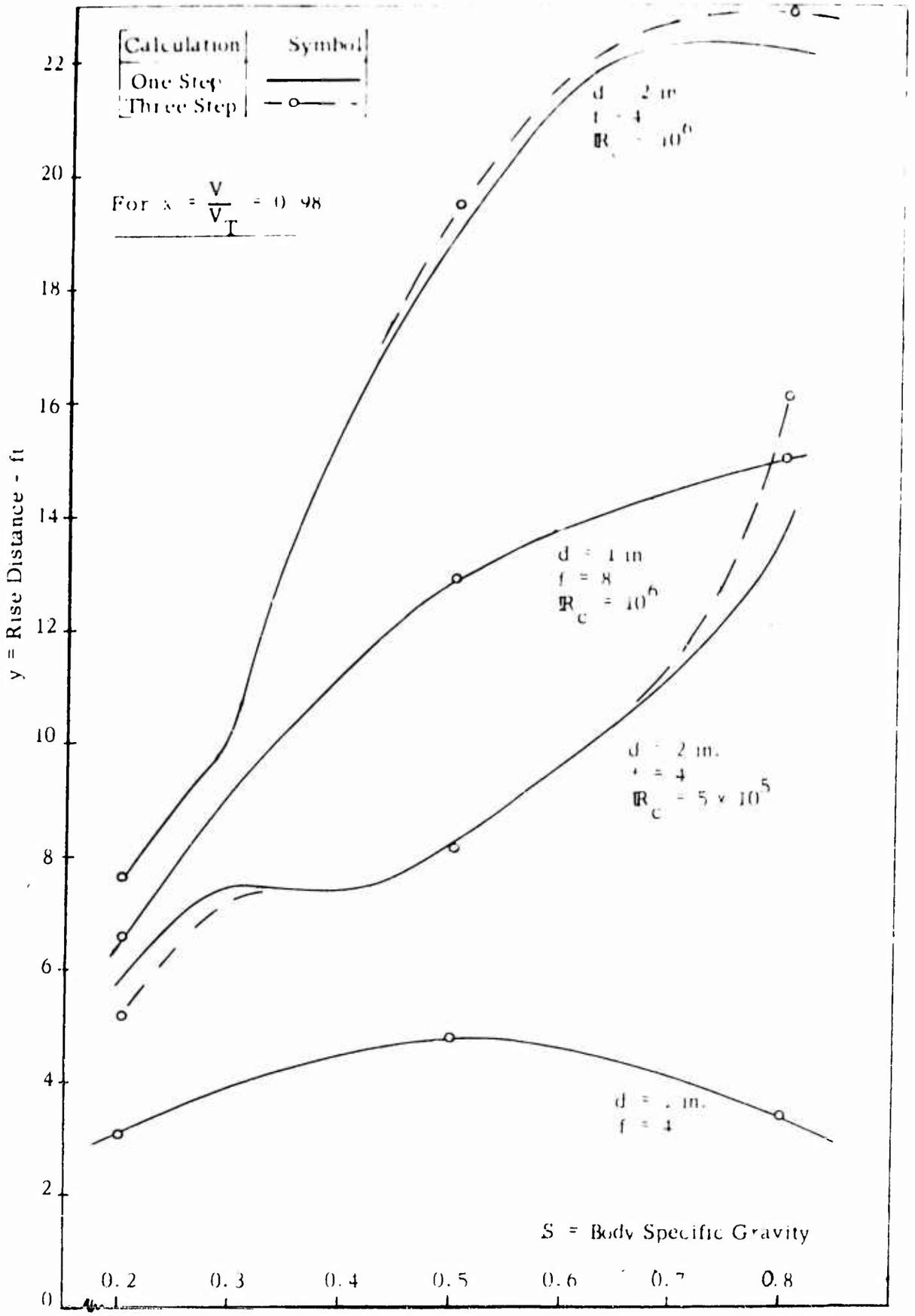

Fig. 13. Calculated Rise Distances for Various Bodies.

The points shown on Fig. 13 were found by the multiple step calculation procedure of Eq. 18a. The necessity of this complicated calculation is subject to question since in some cases the extra terms had little effect. In the case of 2-in. body, the rise distances have been calculated for every tenth change in S over the range plotted. Six of the points were also calculated by the more exact procedure; the agreement is rather good in four cases (errors of 1 to 3 percent). In two cases, however, the one step method is not too good since errors of 10 and 15 percent occurred. Even such errors may not be unreasonable when one considers that the definition of the rise distance (even in terms of $x = 0.98$) is physically vague. In many cases a single step calculation probably suffices.

IV APPROXIMATE ADDED MASS VARIATION IN SURFACE REGION

It is desired to determine the variation in the added-mass coefficient of an elongated body, as it passes through the free surface of a body of water. It is obvious that the virtual mass of the body must decrease as it passes from the denser to lighter medium. One can predict the decrease in added mass of the body and therefore the velocity increase (from momentum analyses) by assuming that on exit all of the momentum represented by the added mass in water must be transferred to the body. As has been noted, this approach does not appear to be too satisfactory.

The details of the change in added mass as the body approaches and then passes through the free surface are also of considerable interest. As noted in Chapter I, theoretical analyses of the occurrences are not simple. This present note presents some approximate analyses of the occurrences as the body passes through the free surface. Although the analyses are crude and quite simplified, it is thought that this approach is of some value in indicating roughly what happens. The analysis is adapted from a water entry or impact analysis proposed by von Karman in 1929 (16) for estimating landing forces on seaplane hulls.

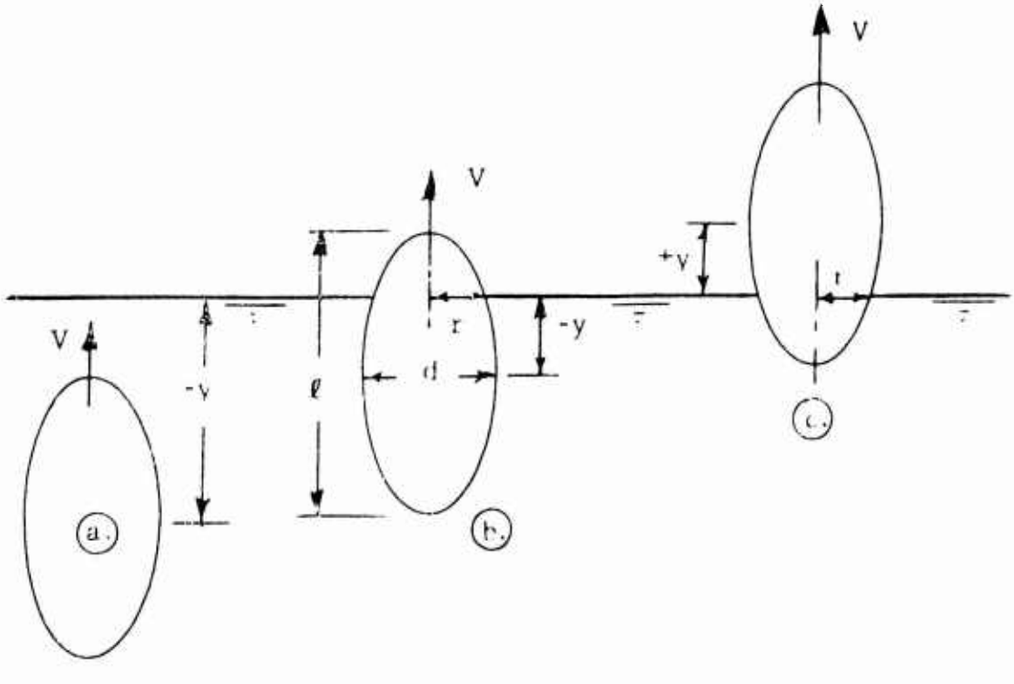

Fig. 14 Body in Various Stages of Exit

IV. 1. Analysis I

A body of the shape considered is sketched in Fig. 14 as it is exiting from the water into air. The body is an ellipsoid of revolution, with length ℓ and diameter d. The coordinate of the centroid is given by y, which is positive when the centroid is out of the water. The radius of the section of the body located at the water surface is indicated by the symbol r. This has the maximum value of d/2. The density of the water is ρ and the density of the air is neglected.

It is assumed that the water surface remains plane as the body passes through it. As y increases in Fig. 14, the added mass of the body must decrease since there is less of it in the water. Following von Karman's two-dimensional approach for motion in the other direction, it is assumed that the added mass is directly given by the radius r, and that it does not depend upon the manner in which r varies with y. The added mass is therefore taken to be that of a sphere of radius r, which is half water and half air. Since the mass of air is neglected, and the added mass of a sphere is one-half its displaced mass of fluid, the added mass of the body is expressed by the following relation

$$M' = \frac{\rho}{4} \cdot \frac{4}{3} \pi r^3 = \frac{\pi}{3} \rho r^3 \tag{19}$$

The added mass is usually expressed as a fraction of the mass of a volume of water equal to the volume $\forall$ of the body. The added mass coefficient is thus

$$k = \frac{M'}{\rho \forall} = \frac{2 r^3}{d^2 \ell} \tag{20}$$

The radius r is related to the axial distance y by the equation

$$\frac{r^2}{d^2} + \frac{y^2}{\ell^2} = \frac{1}{4} \tag{21}$$

substituting this into Eq. 20 yields the result

$$k = \frac{2d}{\ell} (1/4 - y^2/\ell^2)^{1.5} \tag{22}$$

This gives the added mass relation for the body when it is more than half way out of the water.

Application of Eq. 22 to the case when y is negative, i.e., when the body is less than halfway out, leads to an increase in k as the body exits. This, of course, is illogical. The variation of k with distance from the surface should be

such that at large negative values of y the added mass has some constant value. In the present approximation k should start to decrease when the nose of the body touches the free surface ($y = -\ell/2$), should be reduced by one-half when the body is halfway out ($y = 0$), and should reach zero when the tail is just leaving the water surface ($y = +\ell/2$). The solution for k should be symmetrical about the value obtained with $y = 0$. This value is $k_o = d/4\ell$. This symmetry could be obtained by expanding Eq. 22 about this value and letting the extra terms have different signs for the two regions, thus

$$k = \frac{d}{4\ell} \pm \left[-\frac{3}{2}\frac{dy^2}{\ell^3} + \frac{3}{2}\frac{dy^4}{\ell^5} + \frac{dy^6}{\ell^7} + \frac{3}{8}\frac{dy^8}{\ell^9} + \ldots \right] \qquad (22a)$$

where the plus sign after the first term goes with positive y values and the minus sign goes with negative y values. Since the equation is not to apply for numerical values of y/ℓ greater than $1/2$, the convergence is rapid.

The preceding arbitrary modification of the solution to make it symmetrical about the halfway point can be shown to have a rational basis. Consider a body less than halfway out of the water, as in Fig. 14b. In terms of the present approximation it has an added mass coefficient of k'. When this same body is further out of the water, as in Fig. 14c, such that its centroid is as far above the surface as it was below in the previous case, its added mass coefficient is k''. When the body was completely submerged (Fig. 14a) its added mass coefficient is k, which by superposition equals $k' + k''$. This is the assumption upon which Eq. 22a is based.

When Eq. 22a is solved for y equals $-\ell/2$, the following expression is obtained for the added mass coefficient of the submerged body,

$$k_s = \frac{d}{2\ell}$$

Comparison of this submerged coefficient with that given by infinite fluid theory indicates a divergence which increases with fineness ratio ℓ/d. In terms of the present approximation it will be assumed that for $y \lesssim -\ell/2$ the infinite fluid values apply while for $y \gtrsim +\ell/2$ the value of k is zero. The magnitude of the k values given by Eq. 22a are adjusted for all values of y by the needed correction. Thus the present solution, as in Eq. 22a, is utilized only in its mode of variation. The variation in k for motion near the free surface is finally

$$\frac{k}{k_s} = \frac{1}{2} \pm \left[-3\left(\frac{y}{\ell}\right)^2 + 3\left(\frac{y}{\ell}\right)^4 + 2\left(\frac{y}{\ell}\right)^6 + \frac{3}{4}\left(\frac{y}{\ell}\right)^8 + \ldots \right] \qquad (23)$$

The fully submerged value of the added mass coefficient k_s is to be determined from potential fluid theory (as given in Fig. A1), for $\ell/d = 4$, $k = 0.082$ and for $\ell/d = 8$, $k = 0.029$.

IV.2 Analysis II

The above analysis is subject to the objection that the added-mass coefficients of the elongated bodies are being determined as though the bodies were spheres of the same diameter as the body cross section at the free surface. An improved approximation is to calculate the added mass as that of an ellipsoid of revolution of diameter $2r$ and fineness ratio $(\ell/2 - y)/r$ with, of course, only half of it in the water. This approach is only valid for positive values of y, as in the previous case.

When the body is less than halfway out (y negative), the same procedure is followed as for the first analysis. Since it is not possible to express the relation for the added mass coefficient in the form of a simple equation as with Eqs. 21a and 23, the results are presented in the Appendix (Section VIII.6) for two fineness ratios. This second analysis is superior in requiring no correction to k for agreement with the fully submerged added mass coefficient. The approximation does not seem completely satisfactory, however, since the added mass no longer decreases monotonically to zero as the body exits. As apparent in the tabulation k/k_s for the finer body drops below one half before the mid point of the body is reached, but returns to this value and then overshoots for awhile. This is the result of the approximation used, since two segments of the ellipsoid placed end to end do not make another ellipsoid. The single curve shown in Fig. 15 was obtained by ignoring this hump and otherwise averging the results calculated for the two fineness ratios. It is felt to be an adequate approximation.

An even better approximation would be obtained by utilizing anapproximate formula for k, which Landweber and Winzer (2) found for treating bodies more arbitrary than an ellipsoid of revolution. This has not been tried, since the general approach being used is rather crude.

IV.3. Analysis III

Both of the above approximations assume that the variation in added mass occurs only when the body is in contact with the surface. That this may not be so is apparent from Eqs. 2 and 2a and the experimental results obtained in this study (1). The added mass varies as the submerged body approaches the free surface. At low

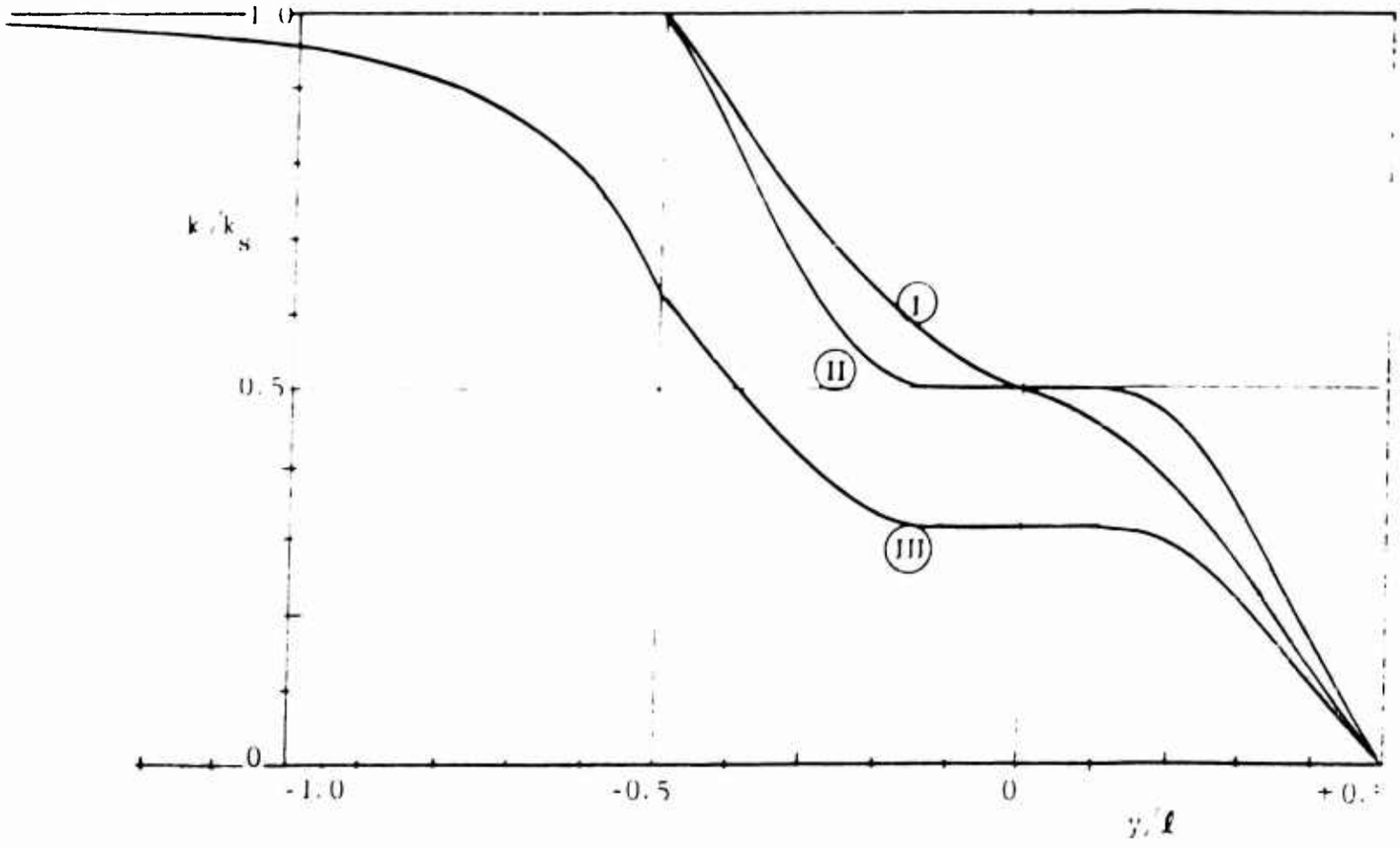

Fig. 15. Added Mass Variation from Several Analyses

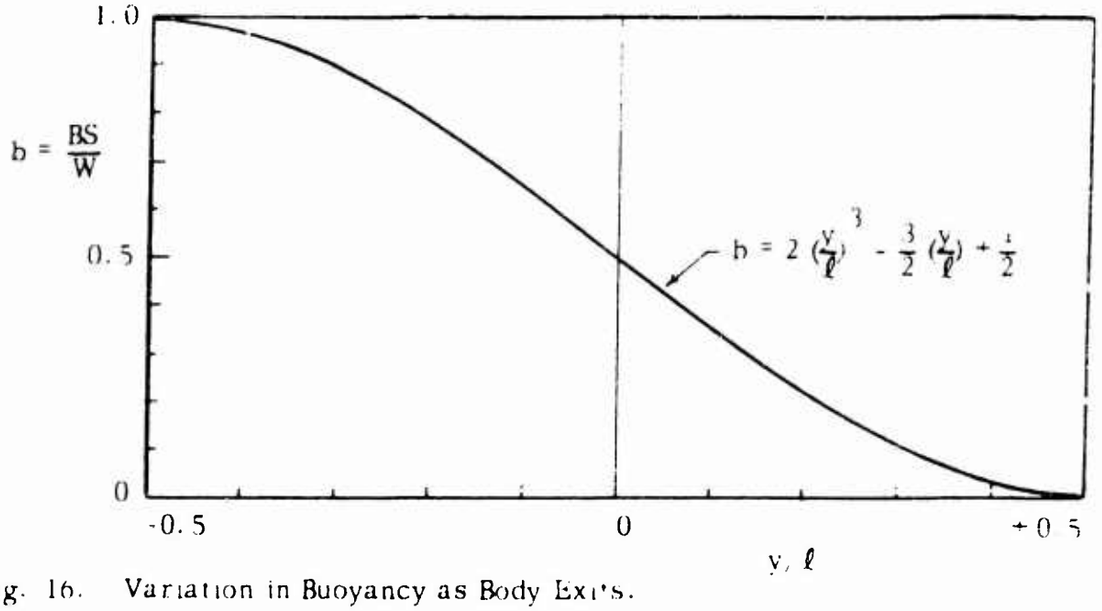

Fig. 16. Variation in Buoyancy as Body Exits.

Froude numbers it increases, at high Froude numbers it decreases to as much as 48 or 50 percent of the submerged value.

Since interest here centers in the higher Froude number range a rational improvement to the previous analyses appears possible by assuming a decrease in k proportional to $(y/\ell)^3$ as the body approaches the surface. When the body nose just touches the surface it will be assumed that k is reduced to 5/8 of k_s. Actually this reduction factor must depend upon the Froude number, however the present assumption appears to be an improvement over that of no variation in k until the surface is contacted. The resultant variation in k/k_s is also presented in Fig. 15 and tabulated in the Appendix.

V. APPROXIMATE VELOCITY AND ACCELERATION EXIT PROFILES

On the basis of the approximate variation found in the previous chapter for the added mass and relations for the velocity drag it is possible to predict the behavior of a body during exit. Of course, the result will be an oversimplified picture of what happens since in reality the exact mode of added-mass-coefficient variation before and during exit is only approximated. In spite of this limitation it is felt that these calculations are of some value in indicating trends and the relative importance of changes in added mass, buoyancy, and drag as the body exits. Furthermore, they may be of even more value when extended to the angle exit case where larger effects may result, since the lateral added-mass coefficients involved are an order of magnitude larger.

V.1. Basic Motion Equations

Consider a body of volume $\forall$, specific gravity S, and added mass coefficient k, moving vertically towards a free surface. The forces acting on the body are buoyance B, weight W and resistance or drag D. Following Eqs. 11 and 14, the equation of motion for the body is

$$B - W - D = \frac{W}{g}\left(1 + \frac{k}{S}\right) a \tag{24}$$

When the body is at terminal velocity $a = 0$ and $B - W = D = D_T$. In the present analysis it is assumed that nothing changes* until the nose touches the free surface. After this B, D, and k change. This leads to a change in velocity indicated by the acceleration

$$\frac{a}{g} = \frac{B - W - D}{W(1 + k/S)} = \frac{b - S - R}{S + k} \tag{25}$$

where $b = BS/W$ is a reduced buoyancy force, varying from unity to zero as the body exits, and $R = DS/W$ is a reduced drag force.

The velocity variation of the body is given as a time integral of the acceleration relation. With the initial condition $V = V_T$ at $t = 0$ (well below the surface) the velocity is

$$V - V_T = \int_0^t a\,dt = g \int_0^t \frac{b - S - R}{S + k}\,dt \tag{26}$$

---

* Except for the Analysis III variation in k.

The acceleration term is zero (except for k - variation III) when the body is below the surface ($t < 0$). A suitable space-time transformation is needed to effect this integration, since b, k, and R (to some extent) are known functions of position of the body in the free surface and not of time. Since the change in V is small, t is proportional to y/V, whence

$$dt = 1/V \; dy \tag{27}$$

and the relation for velocity becomes

$$V - V_T = g \int_0^y \frac{1}{V} \left(\frac{b - S - R}{S + k}\right) dy \tag{26a}$$

The velocity V inside the integral is either assumed constant or the solution performed in stepwise fashion.

It has been noted (cf. (1), p. 15) that Eq. 23 is incomplete when the body is near a surface due to the development of interference forces at the surface. Since these forces are usually not known, the solution to the motion problem must be approached via energy considerations. Up to the point where the body breaks the free surface it is reasonable to assume a constancy in kinetic energy, since the energy dissipated at the surface in waves is probably small. Once the body commences to actually exit the change in potential energy (from the motion of the weight) and the work done by the buoyancy and drag, which now are variables, must be considered. With the assumption of negligible work by the free surface force (negligible energy dissipation at free surface) work-energy considerations yield the following relation

$$(B - D - W)\,\Delta y = \Delta(\text{kinetic energy}) = \Delta\left[\frac{W}{2g}\left(1 + \frac{k}{S}\right) V^2\right]$$

or

$$(B - D - W)\,dy = \frac{W}{g}\left(1 + \frac{k}{S}\right) V\,dV + \frac{WV^2}{2Sg}\,dk$$

whence

$$\frac{dV}{dy} = \frac{B - D - W}{WV(1 + k/S)}\,g - \frac{V}{2S\,(1 + k/S)}\,\frac{dk}{dy}$$

and the following modified form of Eq. 26 results

$$V - V_T = g \int_0^y \frac{1}{V} \left(\frac{b - S - R}{S + k}\right) dy - \frac{1}{2} \int_0^y \frac{V}{(S + k)}\,dk \tag{28}$$

It appears that Eq. 26a is but a first approximation, depending upon the magnitude of the

second term in Eq 28. Inspection suggests that since its relative significance varies as kV^2, this term may thus be quite important for rather blunt bodies at appreciable Froude numbers.

V.2. Relation for Reduced Buoyancy Force

Before calculating the acceleration and velocity variations of the exiting bodies it is desirable to organize information on buoyancy and drag variations in suitable fashion. The relations, $b = b(y/\ell)$ and $R = R(y/\ell)$ are needed. The third variable in Eq. 26 or 28 is $k = k(y/\ell)$ and this is available from the preceeding section.

The relation between $b = BS/W$ and the position of the body in the interface is simply one of geometry. When the body is partly exited, its buoyancy is simply that of the residual submerged volume $\forall'$ times the liquid specific weight. Since $W = S\gamma\forall$, where γ is the specific weight of water and $\forall$ the total volume of the body

$$b = \frac{BS}{W} = \frac{\forall'\gamma S}{S\gamma\forall} = \frac{\forall'}{\forall} \tag{29}$$

From the geometry of the ellipsoid, with the aid of calculus, the volume ratio is given by the relation

$$b = \frac{\forall'}{\forall} = \frac{1}{2} - \frac{3}{2}\frac{y}{\ell} + 2\left(\frac{y}{\ell}\right)^3 \tag{29a}$$

As in previous sections y is the distance of the center of the ellipsoid from the free surface. Equation 28a applies only in the range $-\frac{1}{2} < \frac{y}{\ell} < +\frac{1}{2}$ whence b varies from unity to zero as shown in Fig. 16 (cf. page 39).

V.3. Reduced Resistance Force

The drag depends upon the wetted surface of the body and its velocity through the water. In contrast to the calculations of Chapter II, the wetted or surface area is now a variable. Moreover, it has been noted in the experiments that when the rising body is partly out of the water an appreciable amount of water clings to its surface. Considerations of this later effect will be deferred to the next chapter and for the present it is assumed that the body above the interface is dry. Since air is much less dense than water its drag will be neglected. It is also assumed that the velocity variation of the body during exit is relatively small, so that the drag relation $R = DS/W = D/\gamma\forall$ is a unique function of y/ℓ.

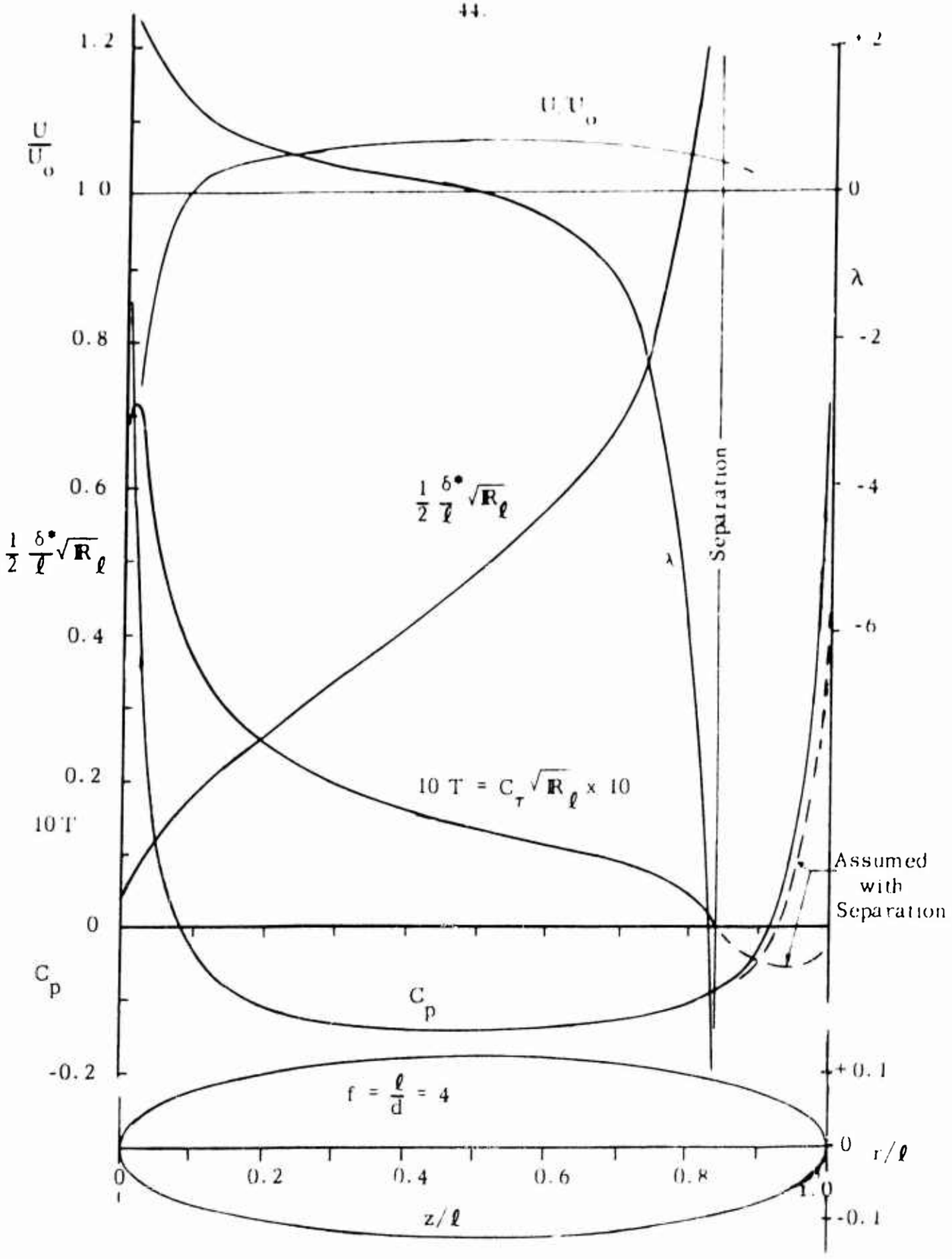

Fig. 17. Laminar Boundary-Layer-Analysis Factors for Ellipsoidal Body.

Determination of the reduced resistance relation involves evaluation of the manner in which the skin friction and pressure portions* of the drag vary along the length of the body. Up to the point of boundary-layer separation the pressure distribution along the body must be close to that obtainable from ideal-fluid theory. The point of separation and skin-friction distribution are determined by the nature of the boundary-layer development along the body. For the laminar boundary layer up to the separation point, this has been determined in general form by Pretsch (17) based on the ideal-fluid velocity distribution along the surface. The calculation of the variation along the surface of the drag contribution of the two factors is thus relatively straight forward, up to the separation point.

Figure 17 depicts the pressure distribution along the body of fineness ratio 4, in terms of the pressure coefficient

$$C_p = \frac{p - p_o}{\frac{\rho}{2} U_o^2} = 1 - \left(\frac{U}{U_o}\right)^2 \tag{30}$$

where

p = pressure along the surface

p_o = reference pressure measured upstream

U = velocity along body surface (just outside the boundary-layer)

U_c (=V) = reference velocity (relative velocity between the body and undisturbed fluid)

ρ = fluid density

The ideal-fluid pressure distribution is symmetrical fore and aft. In the real-fluid case, with separation, the pressures near the tail are somewhat less, as will be discussed later. The variation in skin friction, as taken from Pretsch's work, is indicated by the parameter

$$T = C_T \sqrt{R_\ell} \tag{31}$$

where

---

* Calculation of the pressure drag variation along the ellipsoid, in similar fashion to the present, was given by A. F. Zahm in 1926 (NACA Report 253) both from the ideal-fluid pressure distribution and the pressures measured by Jones (14).

$C_\tau = \dfrac{2\tau_w}{U_o^2}$ = skin friction coefficient

τ_w = local wall skin friction

$R_\ell = U_o \ell / \nu$ = Reynolds number of body in fluid

This parameter T is independent of Reynolds number, except in regard to occurrences after separation For these calculations z is taken as the distance along the major axis from the body nose and r as the lateral coordinate of the surface In terms of ds, the element of length along the surface and the tangent angle, $a = \sin^{-1} dz/ds = \cos^{-1} dr/ds$, the surface forces at any position along the major axis are

$$dD_s = 2\pi r \tau_w \cos a \, ds = 2\pi \tau_w r \, dz$$

$$dD_p = 2\pi r p \sin a \, ds = 2\pi p r \, dr$$

where the subscripts s and p indicate the skin friction and normal pressure portions of the drag. Integration of these over the body will yield the body drag

$$D = D_s + D_p = 2\pi \int_o^\ell \tau_w r \, dz + 2\pi \int_o^{d/2} p r \, dr$$

Reducing this relation to dimensionless form, through division by the dynamic pressure, yields the relation

$$C_D = \frac{2D}{\rho U_o^2 A_\perp} = \frac{8f^2}{\sqrt{R_\ell}} \int_o^1 T \frac{r}{\ell} d\left(\frac{z}{\ell}\right) + 8f^2 \int_o^{1/2f} C_p \frac{r}{\ell} d\left(\frac{r}{\ell}\right) \qquad (32)$$

where $A_\perp$ is the normal area of the body (projected on plane perpendicular to U_o) and f is the length diameter ratio of the body (4 in the case calculated)

For the water-exit calculations it is necessary to evaluate the integrals in Eq. 32 at various positions along the body from 0 to $z/\ell = 1$ Thus for $z/\ell = 0.50$ this will indicate the drag contribution of the front half of the body. Dividing the results of such partial solutions of Eq. 32 by the C_D result, yields the relative contribution to the drag of various portions of the body, forward of any z/ℓ station. The result, calculated with the aid of the C_p and T values of Fig. 17, is shown in Fig 18.

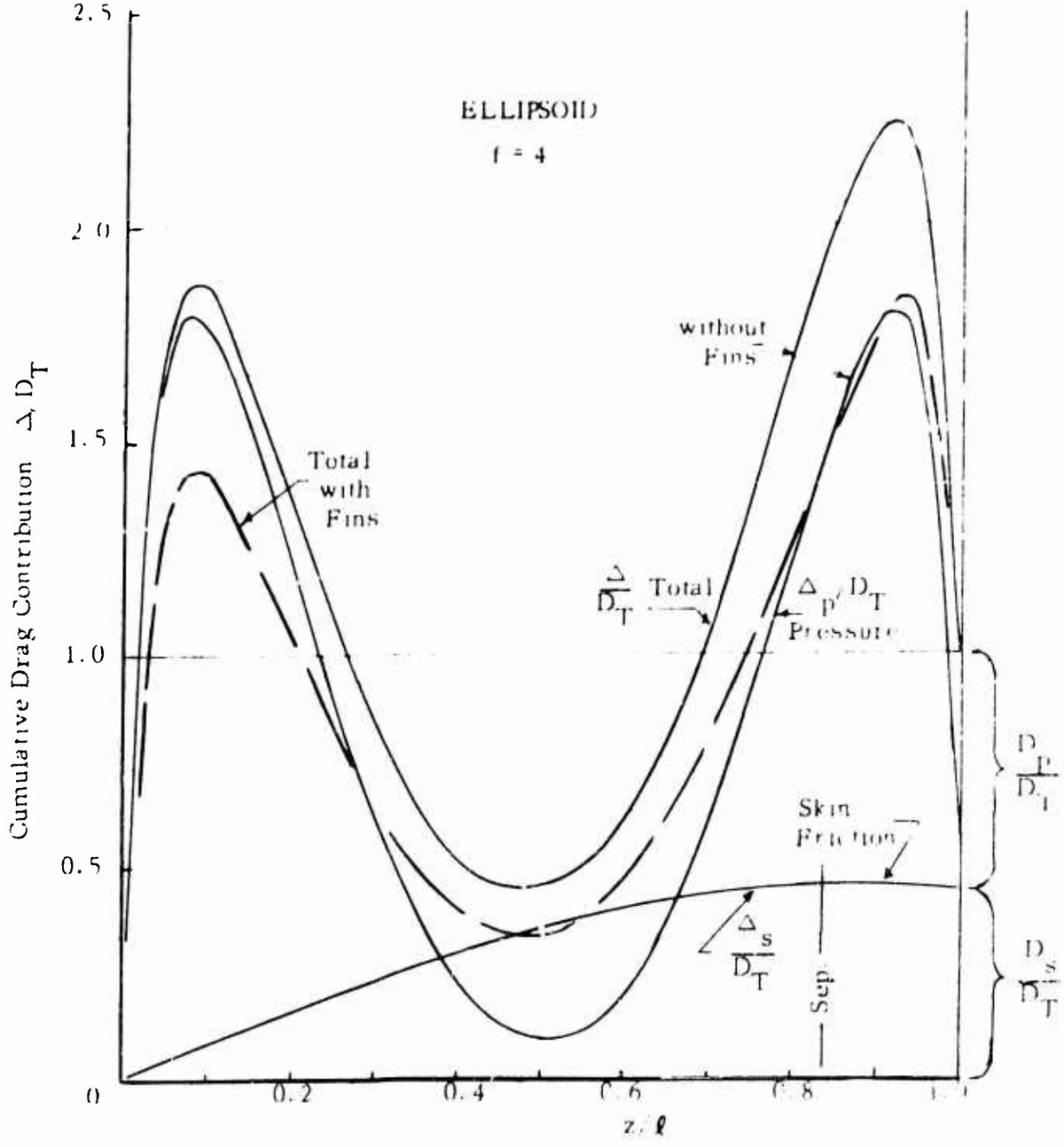

Fig. 18 Calculated Variation in Relative Drag Contributions Along Ellipsoidal Body

From this figure it appears that the total drag contributions of the portion of the body forward of a given station may be as low as 45 percent or as high at 228 percent of the resultant body drag D_T. This variation is primarily due to the pressure. For use in the water-exit calculation, it will be assumed that, as the body exits, the drag contributions of the still-wetted portions remain the same as they were when the body was completely submerged. The residual drag contributions of the wetted portions are thus found by subtracting the contribution indicated by Fig. 18, at the appropriate z/ℓ station, from unity. The relation for R will be presented in Eq. 33.

Before proceeding with the water-exit calculations a few remarks about the post-separation behavior of the flow along the body surface are in order. The boundary-layer analysis gives no clue as to occurrences downstream from the station $z/\ell = 0.838$ where separation is indicated. The flow reversal after separation leads to negative values of T, but these have little influence on the total drag -- most of the skin-friction drag is produced on the front of the body. The assumed T variation near the tail of the body, as depicted in Fig. 17, is felt to be reasonable. The flow behavior after separation has a much more significant effect on the pressure drag. The values for C_D used in the calculations near the tail and shown in Fig. 17 represent a considerable regain in pressure following separation. Since little information on the flow behavior and resultant pressure regain after laminar boundary-layer separation was found in the literature, the regain was adjusted* to yield a reasonable drag coefficient. From Fig. 4 for an $\ell/d = 4$ body without fins and no transition to turbulence effects, the drag coefficient at $R_\ell = 10^6$ is $C_w = 0.0032$. In terms of the fineness ratio of the body C_D is 0.0412 (i.e. $12.87\ C_w$)

The drag contributions of the fins used on the test bodies must still be included. Since these are simple flat plates the calculation is straight forward. In terms of the fin proportions for the 2-in $\ell/d = 4$ body the result is depicted in Fig. 18 as the dashed line. The variation in Δ/D_T is thus from zero to 1.43 to 0.33 at about the midpoint on the body, to 1.92 and back to 1.00 at the tail.

---

* A regain in pressure to a C_p of about 0.45 at the rear stagnation point was required. The effect of the pressure regain on drag is large. Thus the first estimate of a regain to 0.10 yielded a C_D value of 0.0816, nearly twice the value deemed appropriate. The observations of Jones (14) on an f = 4 ellipsoid were particularly suggestive in this regard. He found D_p to be 40 percent of D versus the present result of 55 percent.

For use in the water-exit calculations the factor R is given by the relation

$$R = \frac{D}{\gamma \forall} = \frac{D_T - \Delta}{\gamma \forall} = (1 - \frac{\Delta}{D_T})(1 - S) \qquad (33)$$

where D_T is evaluated from the terminal velocity (below surface influence region) relation of Eq. 8. It should be noted again that changes in the velocity of the body are assumed to be small enough to have negligible effect on R. With D_T varying with velocity to some exponent usually less than 2 and in terms of the experimental velocity changes of the order of 5 percent or less, the error introduced by this approximation is not large.

V.4. Velocity and Acceleration Profile Calculations

Solution of Eq. 28 via stepwise integration with the aid of the relations developed for b, R and k has been carried out for a number of situations. Calculations have been limited to the $f = \ell/d = 4$ ellipsoids for which (cf. Fig. A1) $k_s = 0.0816$.

Figure 19 presents some of the results obtained for a body of specific gravity $S = 0.25$ at a Froude number $F = 8$. These are presented in the same fashion (cf. Fig. 3) as used for the experimental results (1), i.e. as the velocity ratio V/V_T and acceleration a versus y/ℓ, the relative position of the center of the body. Portions of the acceleration profiles are shown dashed in regions where the stepwise integrations were not detailed enough (the increment of calculation $\Delta y/\ell$ was too large) to clearly delineate the mode of variation in a. These curves represent smoothed lines through the calculated values. For the body center below the surface the analytical results bear considerable resemblance to the experimental. Above the surface the second hump in the velocity and acceleration profiles does not appear experimentally. One possible factor (entrained water), which may adjust for this effect, is discussed in the following chapter. The present discussion will therefore be limited to the below surface results. Before leaving the above surface predictions; it is interesting to note that a peak velocity ratio of about 1.19 is predicted, appreciably less than the value 1.33 predicted by the elementary momentum analysis (velocity jump) as indicated by Eq. 1. The below surface peak indicated in Fig. 19 is 1.11 to 1.14, less than the above surface peak.

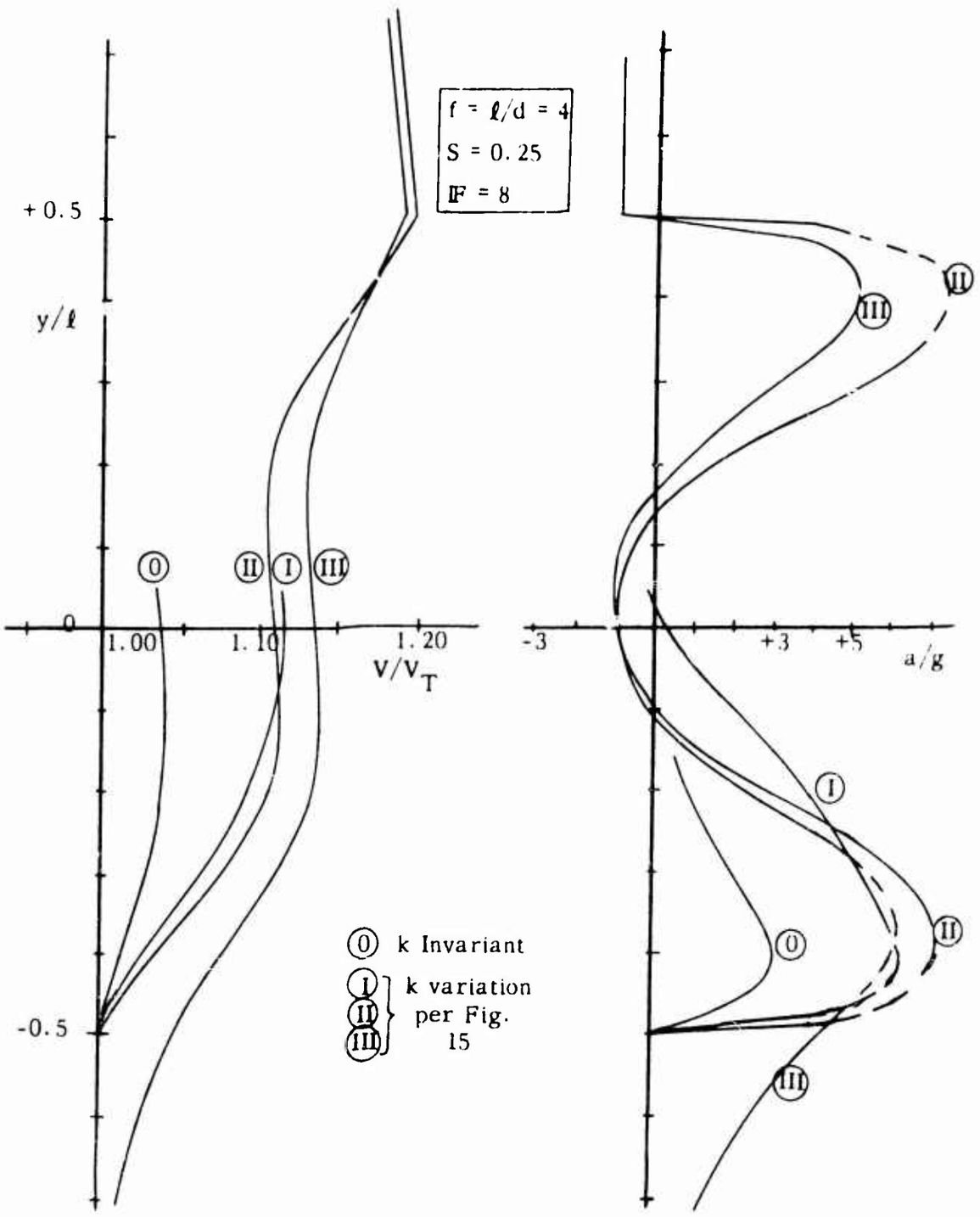

Fig. 19. Calculated Velocity and Acceleration Profiles for Different Variations in Added Mass.

A major objective of the analysis summarized here was to evaluate the relative significance of the various factors entering into the velocity and acceleration profiles. One question, which arises when more exact analysis of the water-exit problem is contemplated, is whether a refined analysis of the variation in added-mass coefficient is worthwhile. It is possible that the effects of buoyancy and resistance changes on the behavior of the exiting body may far outweigh the effects of added-mass changes. A partial answer to this question is evident from the results of the calculations presented in Fig. 19. Here four different variations in added-mass coefficient have been employed in the calculations, namely, that marked 0, with k constant ($k = k_s$), and the I, II, and III variations of Chapter IV. The results based on Analysis III for k approach closest to the experimental results where velocity and accelerations increases are observed to commence before the body nose reaches the surface ($y/\ell = 0.5$). The profiles in this below-surface-contact region result entirely from the second term in Eq. 28. The holding of k invarient throughout the water-exit period (curve 0) considerably reduces the velocity changes and accelerations. Thus the below-surface peak is only 1.042 in this case, rather close to the experimentally observed value. Comparison of the several k relations used for the calculations presented in Fig. 19, thus indicates that the variation in k has a significant effect but that other factors are far from insignificant. Unless much more sudden changes in k appear probable, the exact details of the variation are not important. Thus curves I and II differ little.

The double-humped feature of the calculated profiles results from the variation in the resistance factor R (cf. Eq. 33) and Δ/D_T (cf. Fig. 18) with y/ℓ. Calculation of the profiles which would occur with R invarient are presented in Fig. 20. The velocity and acceleration are seen to peak quickly and then to drop rapidly. The resemblance to the experimental profiles (no second hump, etc.) is closer except that the calculated decelerations become much larger than the observed ones.

The influence of body specific gravity S and Froude number F on the water exit phenomena have been indicated in Chapter I. Thus Eq. 1 suggests that the velocity increase should vary inversely with S. The experiments tend to verify this as well as to indicate a Froude number effect (cf. Fig. 4). Reference (1) shows a rapid increase in Froude number. Calculations of the profiles have also been carried out for two Froude numbers and two specific gravities. The results are presented in Fig. 21 which appears to verify the expected effect of S on the velocity increase as

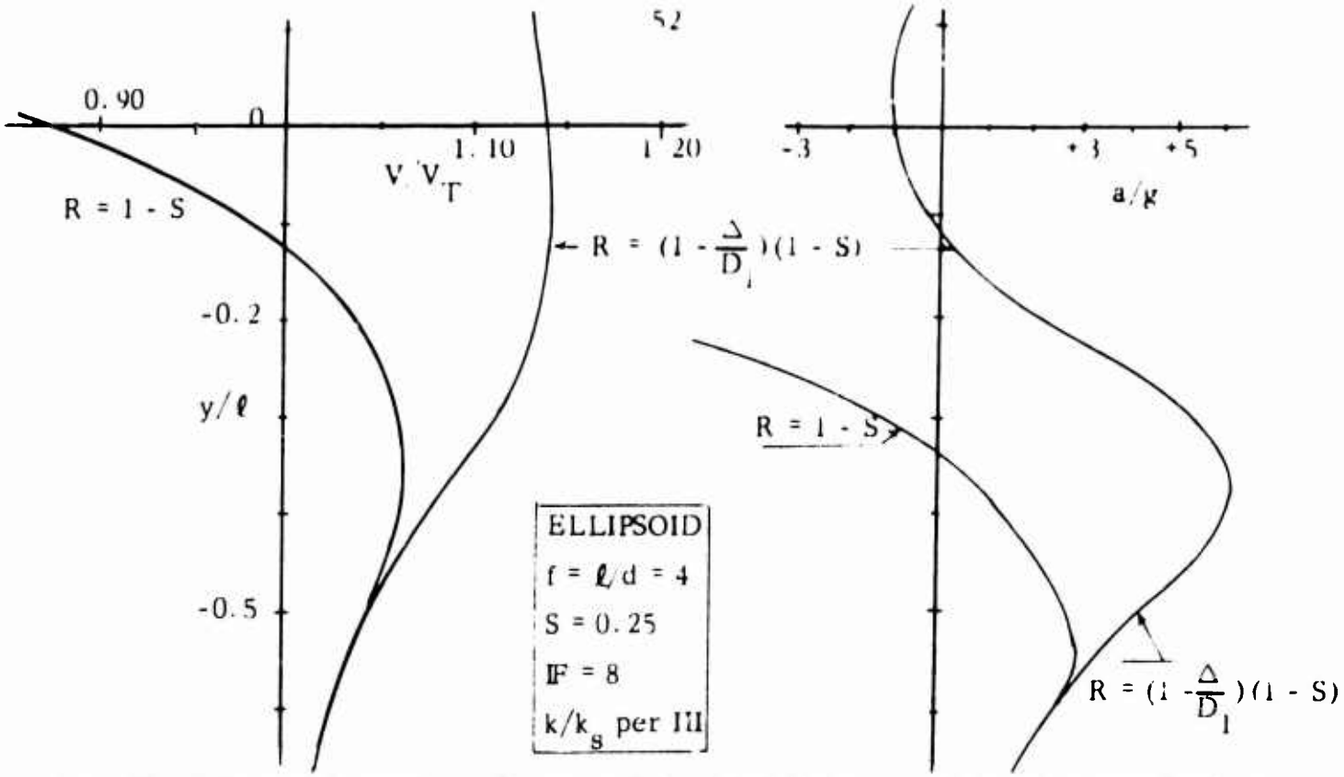

Fig. 20. Effect of Resistance Factor on Calculated Velocity and Acceleration Profiles.

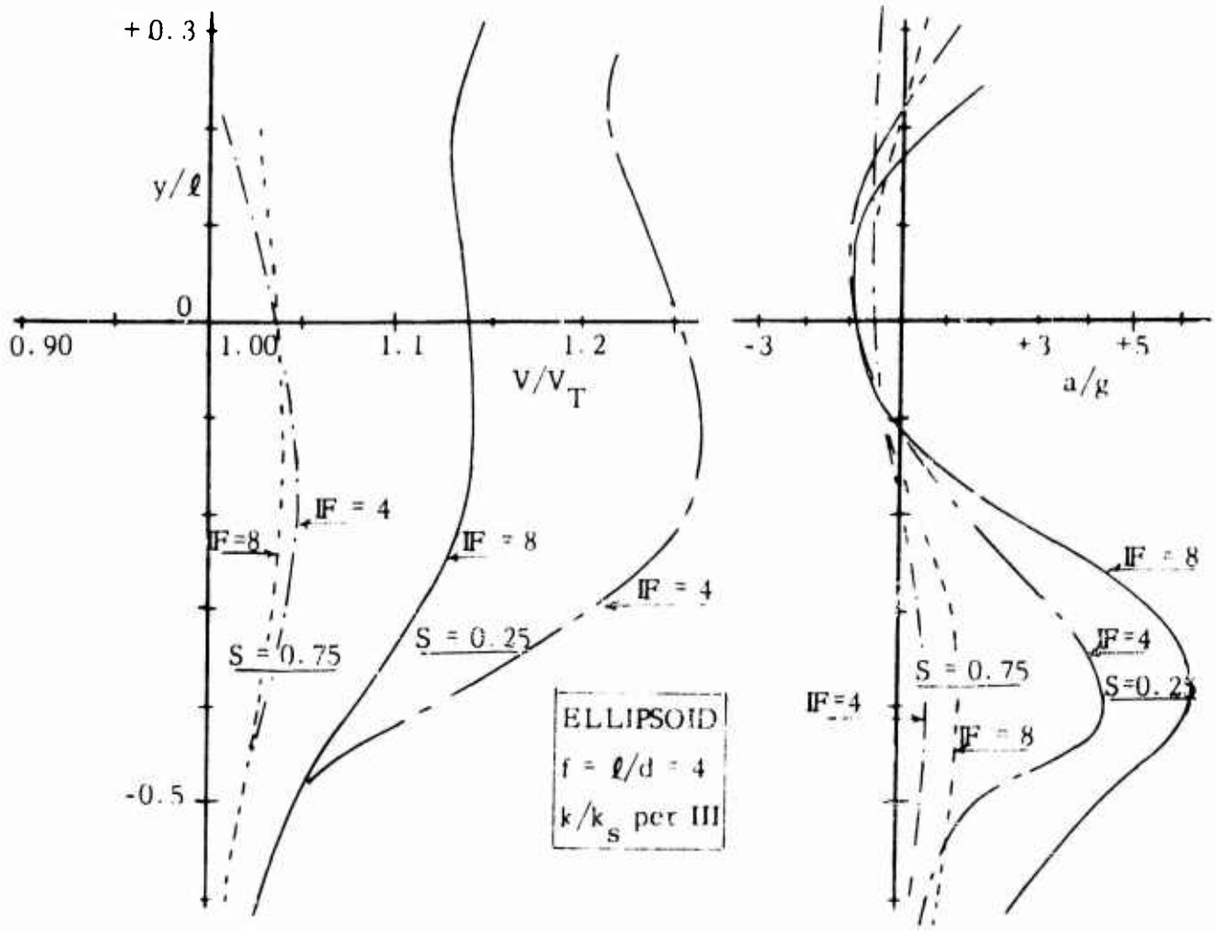

Fig. 21. Effect of Specific Gravity and Froude Number on Calculated Profiles.

well as to indicate an effect of S on the accelerations. The effect of F is not well correlated, however. An increase in acceleration with F is found somewhat as in the experiments but the variation in relative velocity increase with F shown in Fig. 21 is not found experimentally.

The assumption of a lack of Froude number effect on k (cf. Section IV 3) presumably enters here. These calculations have been limited to the $f = \ell/d = 4$ body shape. The major effect of fineness ratio f is a change in the submerged added mass coefficient k_s

VI. CONSIDERATIONS OF ENTRAINED WATER

From the first tests (in November 1956), the experimental phases of this project have indicated that significant amounts of water were entrained by the exiting bodies. Figure 2 indicates this clearly. Crude measurements of this quantity have been reported (1) and the volume was shown to be an appreciable fraction of the volume of the body -- of the same order of magnitude as the added-mass coefficient. It appears probable that this entrained water is associated with the boundary layer on the body. However, the displacement volume of this layer was calculated and found to represent only about 55 percent of the measured entrained water (1). These calculations are presented in more detail in the following section after which they are extended to other scales of motion in an attempt to assess the possibilities of Reynolds-number scaling on entrained water. In the previous chapter mention was made of the possible effect of this entrained water on the water-exit calculations. This factor is introduced into the motion analysis in the final section of this chapter.

VI. 1 Calculation of Displacement Volume

The growth in displacement thickness δ^* along the body may be calculated from the work of Pretsch (17). He presents curves for various ellipsoids depicting the variation in $\sqrt{\mathbb{R}_\ell}\ \delta^*/\ell$ along the body surface. One is shown in Fig. 17, for the $f = \ell/d = 4$ body shape, versus the coordinate z along the body. The displacement volume $\forall^*$ of the boundary layer is found from δ^* by the following integral

$$\forall^* = \int_0^\ell 2\pi r\, \delta^*\, dz$$

In terms of a dimensionless reduced form, appropriate to laminar-boundary-layer analyses, this may be written

$$\frac{\forall^*}{\ell^3}\ \sqrt{\mathbb{R}_\ell} = 2\pi \int_0^1 \frac{\delta^*}{\ell}\ \sqrt{\mathbb{R}_\ell}\ \frac{r}{\ell}\ d\frac{z}{\ell} \qquad (34)$$

where, as before, ℓ is the body length, r the radius of its cross section at any axial distance z from the nose. If the boundary layer did not separate (cf. Section V. 3), Eq. 34 could be integrated to the tail of the body $(z/\ell = 1)$ to yield the displacement-volume relation. However, separation does occur, at a z/ℓ value of about 0.838

(cf. Fig. 17) and in the wake beyond this point $\sqrt{R_\ell}\ \delta^*/\ell$ values are not available from boundary-layer analysis.

The boundary-layer displacement volume up to the separation point is easily calculated from Pretsch's result introduced into Eq. 34. The variation in the integrand with z/ℓ is nearly linear, so the calculation is simple. The boundary-layer displacement volume for a laminar boundary layer on an ellipsoidal body of $f = 4$, to a point $(z/\ell = 0.82)$ just before separation, is found to be

$$\frac{\forall^*_{b\ell}}{\ell^3} = 0.510/\sqrt{R_\ell}$$

or in terms of the body volume $\forall = 0.0327\ \ell^3$ (cf. Fig. A1),

$$\left(\frac{\forall^*}{\forall}\right)_{b\ell} = 15.6\ (R_\ell)^{-1/2} \tag{35}$$

where the subscript ℓ is used to indicate the laminar layer and b the body. Thus, at a Reynolds number of 10^6 the laminar-boundary-layer displacement volume is 1.56 percent of the body volume and at 10^4 it is 15.6 percent.

The wake contribution $\forall^*_w$ to the entrained displacement volume can only be estimated. The behavior of the boundary layer[+] after separation is not well known, as has been noted previously (cf. Section V.3). This flow is often termed the laminar burble, but it rapidly becomes the wake. At Reynolds numbers of interest here (of the order of 10^6) this separated flow will not remain laminar for long. After transition to turbulent flow such separated flows have a tendency to reattach (18). In the present case the separation point is near the tail where the body is so blunt that it has been assumed there is no reattachment. Further consideration of the meager information (18, 19) on the laminar burble suggests that the flow leaves the surface along a tangent. The wake displacement-volume increment was therefore calculated as a conical frustrum tangent to the displacement-thickness contour just before separation. This volume was, of course, reduced by the volume of that portion of the body contained within. The calculation was terminated at the tail. This calculation was made separately for each Reynolds number of interest, since the relative boundary-layer thickness varies with Reynolds number. However, the wake relative-volume contribution $\forall^*_w/\forall$ was essentially a constant. At 10^6 the wake contribution was 0.035 or some 70 percent of the total.

+ Technically after separation the boundary layer may no longer be so termed.

The final item to be included is the viscous displacement volume generated by the four fins. The displacement thickness growth on these is easily computed from flat-plate relations. At a Reynolds number of 10^6 the fin contribution $\forall^*_f/\forall$ is about 0.002 or 4 percent. In general the fin contribution is $2\sqrt{R_\ell}$. At the same Reynolds number (actually 9.7×10^5) the total boundary-layer displacement volume was found to be

$$\frac{\forall^*}{\forall} = \frac{\forall^*_{b\ell}}{\forall} + \frac{\forall^*_w}{\forall} + \frac{\forall^*_f}{\forall} = 0.0528$$

The measured entrained-water volume for the 2-in. body was 1.7 times this. In the case of the 1-in. body (at 2.9×10^5), the measured water was 1.85 times the calculated displacement volume (1). Thus, the correlation between boundary-layer displacement volume and measured entrained water is only fair.

The divergence noted between measured entrained water and calculated boundary-layer displacement volume may be due to any one of several factors. Thus the experimental measurements were crude. They may have included a considerable amount of water in the wake behind the body and this latter was not calculated. Or, surface tension or other fluid properties and phenomena may affect the entrained water.

VI. 2. Displacement Volume for Other Scales

In spite of the uncertainties and apparent inaccuracies in the correlation between entrained water and displacement volume it seems useful to estimate the variation of this volume with the scale of test, on the assumption that this indicates the manner with which the entrained water will change with scale. The experimental program of water exit studies (1) has involved bodies of diameters from 1 to 4 inches. This is a considerable range of sizes and of course there is always the question of extrapolating experimental results to possibly-larger prototype sizes.

The calculations summarized in the preceding section were performed at Reynolds numbers corresponding to test results with the 1-in. and 2-in. bodies. Thus at 2.9×10^5 the calculated $\forall^*/\forall$ value was 0.068 and at 9.7×10^5 it was 0.053. The measured entrained water similarly increased with decrease in scale. The question is, what are the values for the 4-in. body at 3.5×10^6 or some other even larger body? If boundary-layer separation and transition at the higher Reynolds numbers do not enter to complicate the flow pattern, a relation similar to Eq. 34 would provide a simple direct answer. The relative displacement volume would vary inversely as the square

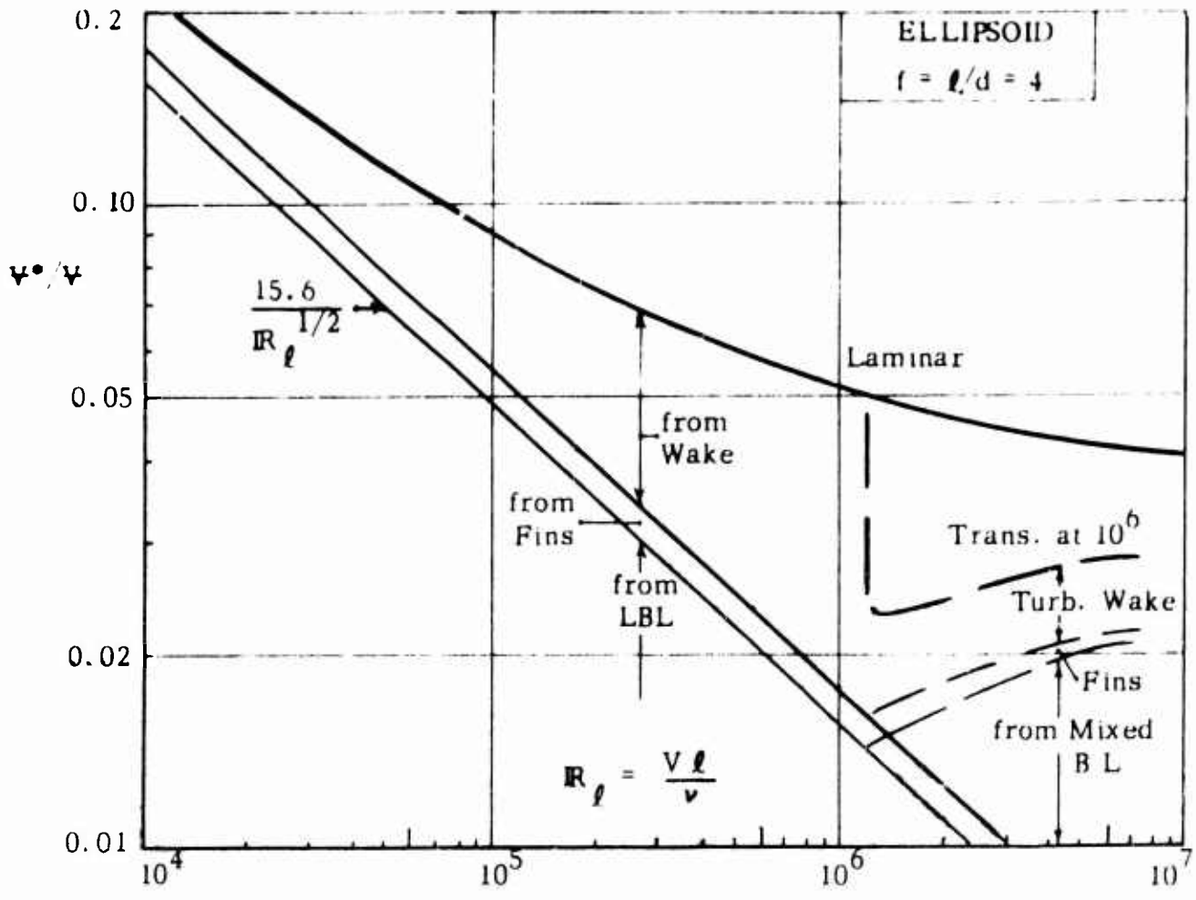

Fig. 22. Variation in Relative Displacement Volume.

root of the Reynolds number*. The wake contribution is not simply calculated once and for all, even without transition. According to Schlichting, although the point of laminar-boundary-layer separation on a given body is invariant with Reynolds number, the angle with which the flow leaves the surface is $\mathbb{R}$ dependent. There appears to be little information on just how this angle varies, however. The wake contribution has thus been evaluated as in the previously mentioned calculations. The relative displacement volume estimate, for the laminar boundary-layer is shown in Fig. 22 as a function of Reynolds number. It is seen to decrease from 22 percent at 10^4 to about

* For Reynolds numbers above 4×10^3, since below this value on a flat plate the Blasius solution no longer is correct.

4 percent at 10^7.

At the higher Reynolds numbers (about 10^6 and above) it becomes increasingly probable that the boundary layer on the body will become turbulent before the laminar separation point is reached. This expectation is indicated by the expected drag coefficient curves of Fig. 5, with some experimental verification shown in Fig. 9. The turbulent boundary layer being more resistant to separation, transition will thus lead to a lower wake contribution to the boundary-layer displacement volume. Since this term represents 70 or more percent of the total at the higher Reynolds numbers, the effect of transition in reducing the displacement volume is considerable.

On the basis of a transition (to turbulent boundary layer) Reynolds number of 10^6 the displacement volume has been estimated at body Reynolds numbers of 2×10^6 and 4×10^6. The calculation is based on use of the Karman momentum-integral equation in step-wise calculation from the transition point. The method used is essentially that given by Granville (12) except that corrections were introduced into the boundary-layer shape parameter and skin friction following the work of Ross (20). Separation was indicated at a z/ℓ value of about 0.95, in contrast to the laminar separation point of 0.838. This led to a considerable reduction in the wake contribution, while the boundary-layer portion is higher, as may be seen in Fig. 22. As suggested in the figure, at Reynolds number above 4×10^6, the displacement volume must reach a peak value and then commence to decrease, after the boundary layer on the whole length of the body becomes turbulent. The sudden drop in $\forall^*/\forall$ at about 1.2×10^6 occurs when the transition point changes from being in the separated flow to being on the body and the separation is then delayed.

Referring these predictions of displacement volume to the actual water-exit test conditions, it is notable that for the 4-in. body tested (at $\mathbb{R}_\ell = 3.46 \times 10^6$) $\forall^*/\forall$ has a calculated value of 2.7 percent versus 5.2 percent for the 2-in. body (at 10^6) and 6.7 percent for the 1-in. body (at 3×10^5). Whether this properly represents or indicates the entrained water or not, it is obvious that a considerable scale effect does occur. This is particularly so at sizes above the 2-in. body in association with boundary-layer transition effects.

VI.3. Entrained Water Effect on Exit Profiles

With an amount of water exiting with the body of about the same value as the added-mass coefficient a considedable modification of the exit behavior is expected. The question of whether this viscous displacement volume simply increases the added

mass coefficient k, involves consideration of unsteady boundary-layer behavior. At exit however, the velocity changes are small and a considerable amount of water is observed to exit with the body. It will here be assumed that this displacement volume actually clings to the body during the entire exit phase. It has been observed in the motion pictures that, when the body is most of the way out of the water, some water commences to roll down and off the body. This suggests that the boundary-layer displacement water does cling to the body during most of the exit phase. An attempt to evaluate the effect of this water on the calculated velocity and acceleration profiles (cf. Section V. 4) has been made and will be presented in the following paragraphs.

It is assumed that the boundary-layer displacement volume clings to the body and exits with it. This implies that, although the buoyancy change is the same during exit, the mass of body plus water exiting is larger; also while the boundary layer is thin enough for the variations in pressure-drag contributions to be the same, the frictional-drag contribution will not vary as the body exits. Thus considerable change is introduced into the several terms in the equations leading up to Eq. 28, particularly R and W. Splitting R into pressure and skin friction parts R_p and R_s with the latter invarient with y/ℓ and introducing the relative displacement volume $v^* = \forall^*/\forall$ into appropriate places in the several terms, Eq. 28 now appears as

$$V - V_T = g\int \frac{1}{\bar{V}} \left(\frac{b - R_p - R_s - S - v^*}{(1 + v^*/S)(S + k)} \right) dy - \frac{1}{2}\int \frac{V}{(S + k)}\, dk \qquad (28a)$$

The numerator of the bracketed term in the first integrand contains the extra term v^* and only $b - R_p$ is a function of body position at the free surface. The second integral is not changed at all. The $b - R_p$ term is available from Fig. 16 for b and Fig. 18 for R_p. This latter term is 42 percent of the total drag or

$$R_p = 0.42\,(1 - \Delta_p/D_T)\,(1 - S) \qquad (33a)$$

where Δ_p/D_T is found from the pressure curve of Fig. 18 multiplied by the factor $0.763 = 1/1.31$, a correction for the fact that this pressure curve is presented as a fraction of the bare body drag and the fins added 31 percent to the bare body drag. The R_s term, representing 58 percent of D_T is simply $0.581\,(1 - S)$, a constant.

Velocity and acceleration profiles have been calculated on this new basis in the same stepwise fashion as used previously (cf. Section V. 4). Results are presented in Fig. 23, in comparison with the previous results for one Froude number and body density. The below-surface-contact behavior is naturally the same as found previously

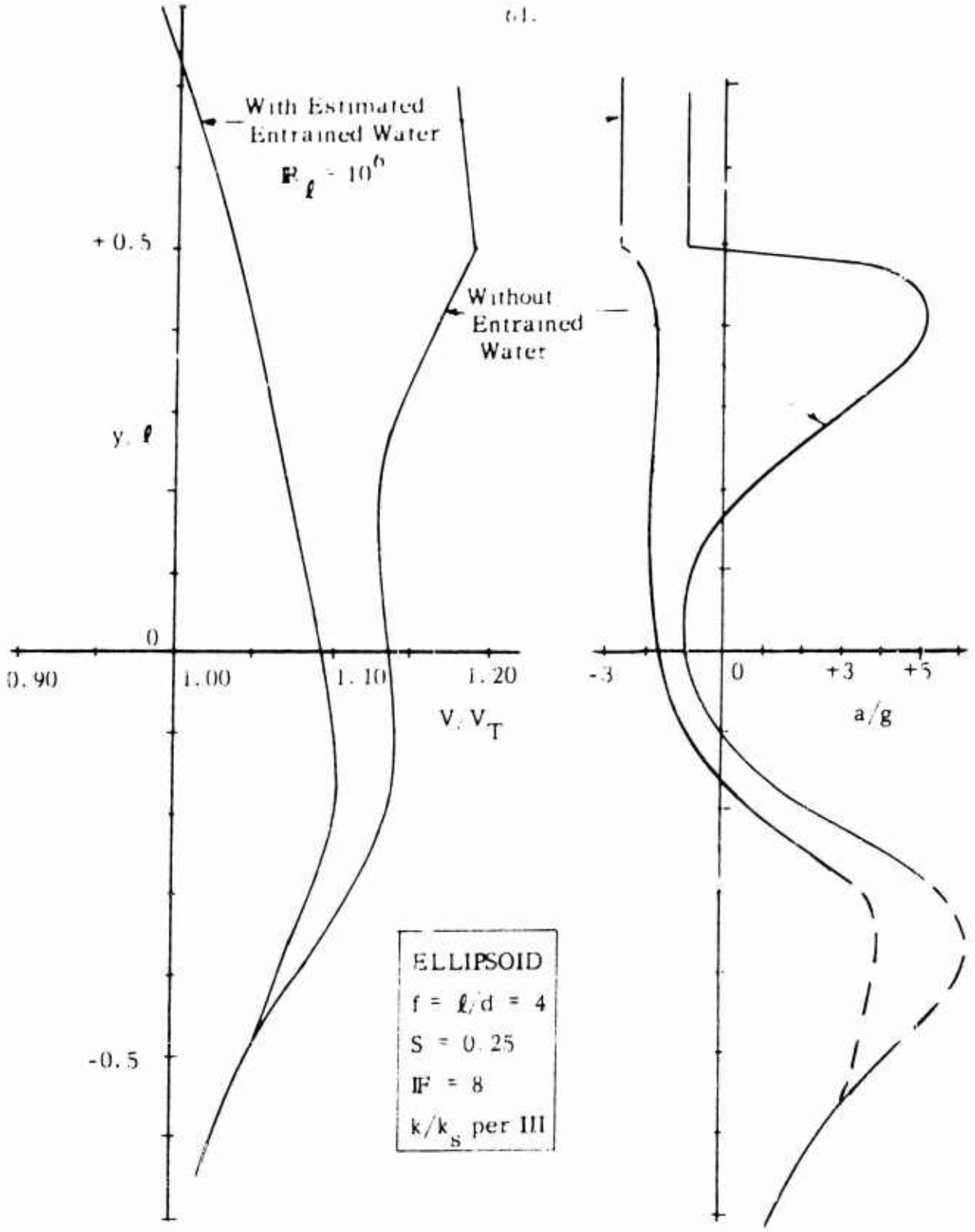

Fig. 23. Calculated Exit Profiles With and Without Estimated Wated Entrainment.

since this results only from the second integral of Eq 28 which is not changed An appreciable reduction in the velocity jump and peak acceleration is seen to result from the water entrainment effect. Furthermore the second peak in velocity and acceleration has also disappeared. The calculated profiles thus more closely resemble those observed (cf. Fig. 3). The discrepancy is now more one of degree A greater entrained water effect could lower the calculated velocity profiles in the regions $-0.2 < y/\ell$ until rather good agreement with experiment is found. The question of the absolute accuracy of the entrained water calculations as the boundary layer displacement volume, in light of the experimental measurements, has already been discussed in Section VI. 1.

Further refinement in the calculation of the profiles seems inappropriate at this time. These last calculations have definitely shown a significant and appreciable effect of the water entrainment on the profiles. If this entrained volume varies with the scale of test (as indicated by Reynolds number) in the fashion suggested by the volume calculations summarized in Fig. 22, then Reynolds number scaling also influences water exit.

VII REFERENCES

1. M. E. Clark and J. M. Robertson, "A Study of the Kinematics of Buoyant-Body Water Exit", TAM Dept. Report 145, University of Illinois, April 1959.

2. L. Landweber and A. Winzer, "A Comparison of the Added Masses of Streamlined Bodies and Prolate Spheroids", Schiffstecknik, Bd. 3, 1955-56, p. 180-183.

3. H. Lamb, "Hydrodynamics", 6th Edition, Cambridge University Press, 1932, American Edition, Dover, 1945.

4. L. M. Milne-Thompson, "Theoretical Hydrodynamics", 3rd Edition, MacMillan, 1955.

5. G. Birkhoff, "Hydrodynamics", Princeton University Press, 1950; Dover Edition, 1955, p. 153.

6. Th. von Karman, "Turbulence and Skin Friction", Jour. Aero. Sci., Vol. 1, 1934, p. 1-20.

7. C. B. Millikan, "Boundary Layer and Skin Friction of a Figure of Revolution", Trans. ASME, Vol. 54, 1932, (APM-54-3), Part I, p. 29-43.

8. H. L. Dryden and A. M Kuethe, "Effect of Turbulence in Wind Tunnel Measurements", NACA Report 343, 1930.

9. N. B Moore, "Application of Karman's Logarithmic Law to Prediction of Airship Hull Drag", Jour. Aero Sci., Vol 2, January 1935, p. 32-34.

10. S. Goldstein, editor, "Modern Developments in Fluid Dynamics", Oxford University Press, 1938, p. 505-519.

11. K. E. G. Wieghardt, "On a Simple Method for Calculating Laminar Boundary Layers", Aero. Quarterly, Vol. V, May 1954, p. 25-38.

12. P. S. Granville, "The Calculation of the Viscous Drag of Bodies of Revolution", David Taylor Model Basin, Report 849, July 1953.

13. S. F. Hoerner, "Aerodynamic Drag", 1951 (book published by author).

14. R. Jones, "The Distribution of Normal Pressures on a Prolate Spheroid", British Aero. Res. Comm., R and M 1061, December 1925.

15. J. M. Robertson, J. C. F. Chow and M E. Clark, "Transition Stimulation for Terminal Velocity Reduction in Water Exit Studies", TAM Dept. Report 152, University of Illinois, November 1959.

16. Th. von Karman, "The Impact on Seaplane Floats During Landing", NACA TN 321, 1929.

17. J. Pretsch, "Die Laminare Reibungschicht an Elliptischen Zylindern und Rotationsellipsoiden bei Symmetrischer Umstromung", Luftfahrt-Forschung, Vol. 18, December 1941, p. 397-402.

18. W. J. Bursnall and L. K. Loftin, "Experimental Investigations of Localized Regions of Laminar-Boundary Layer Separation", NACA TN 2338, 1951.

19. G. B. Schubauer, "Air Flow in a Separating Laminar Boundary Layer", NACA Report 527, 1935; "Air Flow in the Boundary Layer of an Elliptic Cylinder", NACA Report 652, 1939.

20. D. Ross, "A Physical Approach to Turbulent-Boundary Layer Problems", Trans. ASCE, Vol. 121, 1956, p. 1219-1240.

VIII APPENDIX

VIII. 1. List of Symbols Used

a	acceleration of body, fps^2
a	as a subscript, indicates air
a	$= A_w / \ell d$ - body surface area related to normal dimensions of body
A_w	wetted or surface area of body, ft^2
A_f	fin area, ft^2
$A_\perp$	normal or projected area, ft^2
b	$= BS/W$ - reduced buoyancy force
B	buoyancy force of submerged body, lbs.
C_w	drag coefficient based on A_w, cf. Eq. 3
C_F	flat-plate friction coefficient
C_p	pressure coefficient, cf. Eq. 30
C_τ	local skin-friction coefficient
d	diameter of body, inches or feet
D	body drag, lbs.
D_T	body drag in infinite fluid at terminal velocity
D_s	body drag due to skin friction
D_p	body drag due to pressure
f	$= \ell/d$ - fineness ratio of body
IF	$= V/\sqrt{gd}$ - Froude number
g	gravitational acceleration, $32.2\ fps^2$
k	added-mass coefficient
k_s	added-mass coefficient for body submerged in infinite fluid, Chapter IV, V
K	coefficient in power-law relation for drag, cf. Eq. 12
ℓ	length of body, ft.
M	mass of body, slugs
M'	added mass of body, slugs
n	exponent in power-law relations for drag, cf. Eq. 12
p	pressure along body surface, psf
p_o	reference or ambient pressure ahead of body, psf
r	radius of body (perpendicular to major axis) at any point, ft
R	$= DS/W$ - reduced drag factor, cf. Chapter V

$\mathbb{R}_\ell$	$= V\ell/\nu$ - Reynolds number based on body length
S	specific gravity of body = ratio of body weight to that of equal volume of water
t	time, seconds
T	$= C_\tau \sqrt{\mathbb{R}_\ell}$ - reduced laminar friction coefficient
U	velocity along body surface just outside boundary layer (potential velocity), fps
U_o	= V - relative velocity of body through fluid, fps
v	$= \forall/\ell^3$ - body volume related to length cubed
v^*	$= \forall^*/\forall$ - relative displacement volume
V	velocity of body, fps
V_T	terminal velocity of body, fps
$\forall$	volume, usually of or pertaining to body, ft^3
$\forall^*$	boundary-layer (etc.) displacement volume on body ft^3
w	as a subscript, indicates water except in Section V.3
W	$= \gamma S V$ - weight of body, lbs.
x	V/V_T - relative velocity in Chapter III
y	position of center of body relative to free surface, ft (negative when below surface, positive above)
Y	$yg/a\beta V_T^2$ - rise distance parameter in Chapter III
z	position along major axis of body, measured from nose, ft
a	$= 1 + k/S$
α	surface tangent angle
β	$= S/(1 - S)$
γ	fluid specific weight, lbs/ft^3
δ^*	boundary-layer displacement thickness, ft
Δ	portion of drag developed up to any particular z position, lbs.
ν	fluid kinematic viscosity, ft^2/sec
ρ	fluid density, $slugs/ft^3$
τ_w	wall skin-friction coefficient

VIII. 2. Characteristics of Prolate Ellipsoids

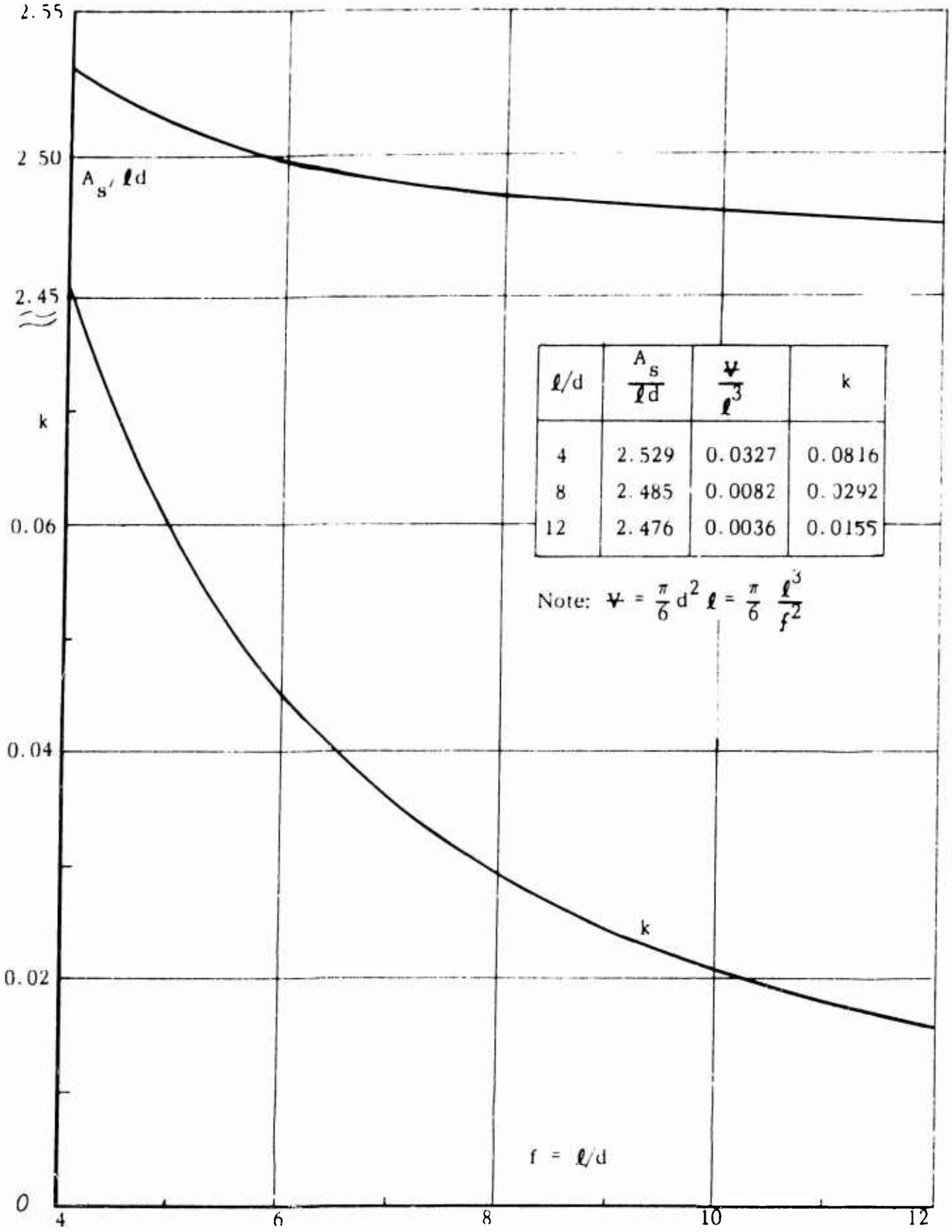

ℓ/d	$\frac{A_s}{\ell d}$	$\frac{\forall}{\ell^3}$	k
4	2.529	0.0327	0.0816
8	2.485	0.0082	0.0292
12	2.476	0.0036	0.0155

Note: $\forall = \frac{\pi}{6} d^2 \ell = \frac{\pi}{6} \frac{\ell^3}{f^2}$

Fig. A1. Surface Areas, Volumes and Added Mass Coefficients of Prolate Ellipsoids.

VIII 3 Table of Body Drag Laws

Fineness Ratio ℓ/d	$\mathbb{R}_{crit}$ (flat plate)	Exponent in Eq. 12 n	$\mathbb{R}$ Limits		Drag Coefficient C_w	Notes
			Min.	Max.		
4	10^6	1.85	1×10^4	8.9×10^4	$0.084\ \mathbb{R}^{-0.15}$	No Fins
		1.30	8.9	42	$44\ \mathbb{R}^{-0.70}$	"
		1.50	42	99	$3.3\ \mathbb{R}^{-0.50}$	"
		2.12	99	330	$0.00066\ \mathbb{R}^{0.12}$	"
		2.00	330	1000	0.004	"
8	10^6	1.60	1×10^4	5.8×10^4	$0.70\ \mathbb{R}^{-0.40}$	No Fins
		1.50	5.8	89	$2.1\ \mathbb{R}^{-0.50}$	"
		2.30	89	260	$0.000036\ \mathbb{R}^{0.30}$	"
		2.00	260	1000	0.003	"
4	10^6	1.80	1×10^4	10×10^4	$0.182\ \mathbb{R}^{-0.20}$	With Fins
		1.25	10	44	$102\ \mathbb{R}^{-0.75}$	$(A_f/A_w = 0.25)$
		1.60	44	110	$108\ \mathbb{R}^{-0.40}$	$(\ell_f/\ell = 0.16)$
		2.00	110	600	0.0042	"
8	10^6	1.56	1×10^4	11×10^4	$1.39\ \mathbb{R}^{-0.44}$	With Fins
		1.50	11	110	$2.8\ \mathbb{R}^{-0.50}$	$(A_f/A_w = 0.13)$
		2.35	110	230	$0.000021\ \mathbb{R}^{0.35}$	$(\ell_f/\ell = 0.08)$
		2.00	230	500	0.0035	"
4	5×10^5	1.80	1×10^4	10×10^4	$0.182\ \mathbb{R}^{-0.20}$	With Fins
		1.25	10	42	$102\ \mathbb{R}^{-0.75}$	"
		2.25	42	89	$0.00024\ \mathbb{R}^{0.25}$	"
		1.8	89	1000	$0.115\ \mathbb{R}^{-0.20}$	"
8	5×10^5	1.56	1×10^4	11×10^4	$1.39\ \mathbb{R}^{-0.44}$	With Fins
		1.50	11	56	$2.8\ \mathbb{R}^{-0.50}$	"
		2.30	56	100	$0.000071\ \mathbb{R}^{0.30}$	"
		2.00	100	280	0.0044	"
		1.80	280	1000	$0.085\ \mathbb{R}^{-0.20}$	"

VIII Rise Distance Parameter Verses Drag Law Exponent

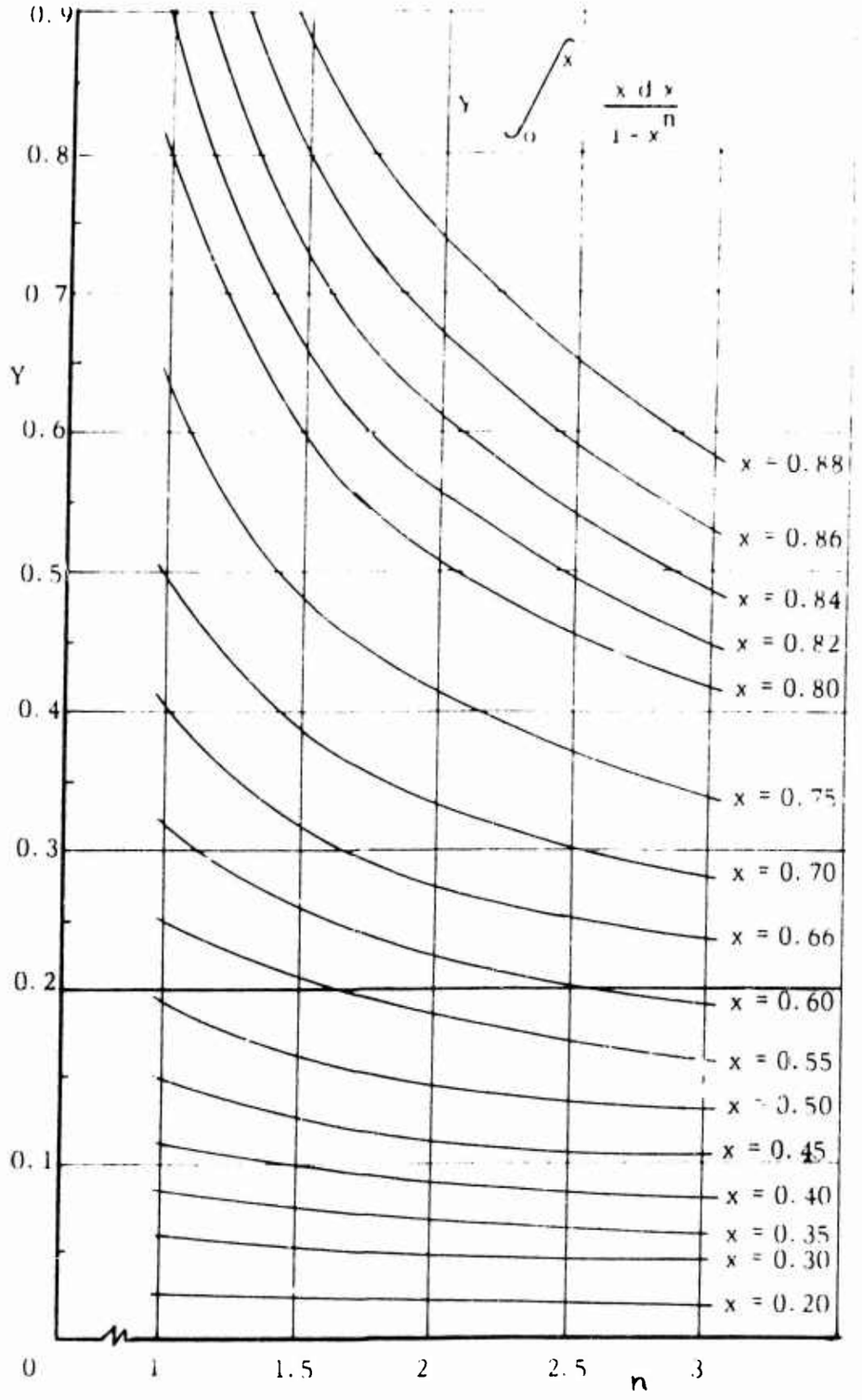

Fig. A2. Rise Distance Equation Solution -- for x up to 0.88

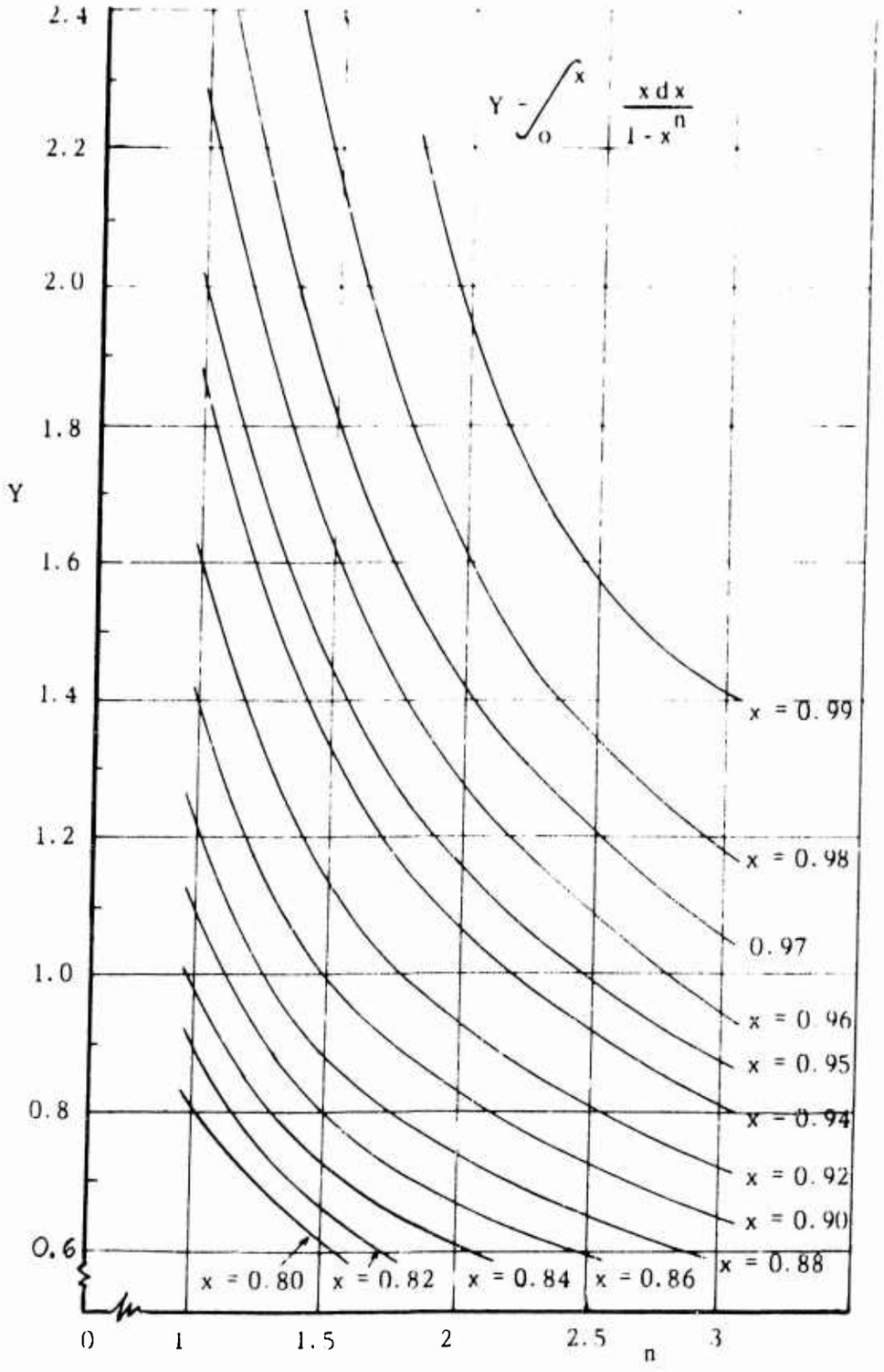

Fig. A3. Rise Distance Equation Solution -- for x from 0.80 to 0.99.

VIII. 5. Table of Numeral Solutions of Rise Distance Equation

values of $Y = y\, g\, a\beta\, V_T^{\,2}$ vs x and n

x \ n	1.0	1.5	2.0	2.5	3.0
0	0	0	0	0	0
0.05	~0.001	0.00126	- - - -	0.00125	- - - -
0.10	0.005	0.005	0.005	0.005	0.005
0.20	0.023	0.02109	0.0205	0.0202	0.0194
0.30	0.057	0.0498	0.0470	0.0460	0.045
0.40	0.111	0.096	0.087	0.0838	0.0813
0.50	0.193	0.162	0.144	0.1362	0.1313
0.60	0.316	(0.2316)*	0.223	0.202	0.1915
0.70	0.504	0.3906	0.3365	0.304	0.287
0.80	0.809	0.6067	0.511	0.4494	0.421
0.90	1.403	0.9932	0.8305	0.7702	0.650
0.95	2.046	1.443	1.1635	0.9903	0.879
0.98	2.932	2.2827	1.6145	1.3454	1.185
0.99	3.615	- - - -	1.958	- - - -	1.414
1.00	∞	∞	∞	∞	∞

* for x = 0.58

VIII. 6. Variation in Added Mass Ratio by Various Analyses

y/ℓ	k/k$_s$ by Analysis I	k/k$_s$ by Analysis II			k/k$_s$ by Analysis III
		ℓ/d = 4	ℓ/d = 8	smoothed	
-1.75	1.000	1.000		1.000	0.994
-1.50	1.000	1.000		1.000	0.986
-1.25	1.000	1.000		1.000	0.976
-1.00	1.000	1.000		1.000	0.953
-0.875	1.000	1.000		1.000	0.930
-0.750	1.000	1.000		1.000	0.888
-0.625	1.000	1.000		1.000	0.808
-0.500	1.000	1.000	1.000	1.000	0.625
-0.375	0.836	0.791	0.775	0.783	0.490
-0.250	0.674	0.583	0.575	0.579	0.362
-0.125	0.556	0.500	0.469	0.500	0.313
0.00	0.500	0.500	0.500	0.500	0.312
+0.125	0.445	0.500	0.524	0.509	0.312
+0.250	0.326	0.404	0.425	0.415	0.260
+0.375	0.1647	0.208	0.225	0.216	0.135
+0.500	0.000	0.000	0.000	0.000	0.000